



**HAL**  
open science

# Large-scale analysis and computer modeling reveal hidden regularities behind variability of cell division patterns in *Arabidopsis thaliana* embryogenesis

Elise Laruelle, Katia Belcram, Alain Trubuil, Jean-Christophe Palauqui,  
Philippe Andrey

► **To cite this version:**

Elise Laruelle, Katia Belcram, Alain Trubuil, Jean-Christophe Palauqui, Philippe Andrey. Large-scale analysis and computer modeling reveal hidden regularities behind variability of cell division patterns in *Arabidopsis thaliana* embryogenesis. *eLife*, 2022, 11, pp.e79224. 10.7554/eLife.79224 . hal-04301574

**HAL Id: hal-04301574**

**<https://hal.inrae.fr/hal-04301574>**

Submitted on 29 Mar 2024

**HAL** is a multi-disciplinary open access archive for the deposit and dissemination of scientific research documents, whether they are published or not. The documents may come from teaching and research institutions in France or abroad, or from public or private research centers.

L'archive ouverte pluridisciplinaire **HAL**, est destinée au dépôt et à la diffusion de documents scientifiques de niveau recherche, publiés ou non, émanant des établissements d'enseignement et de recherche français ou étrangers, des laboratoires publics ou privés.

1 Large-scale analysis and computer modeling reveal  
2 hidden regularities behind variability of cell division  
3 patterns in *Arabidopsis thaliana* embryogenesis

4 Elise Laruelle<sup>1,2</sup>, Katia Belcram<sup>1</sup>, Alain Trubuil<sup>2,\*</sup>,  
Jean-Christophe Palauqui<sup>1,\*</sup> and Philippe Andrey<sup>1,\*</sup>

5 11 March 2022

6 (1) Université Paris-Saclay, INRAE, AgroParisTech, Institut Jean-Pierre Bourgin (IJPB), 78000,  
7 Versailles, France

8 (2) MaIAGE, INRAE, Université Paris-Saclay, 78352 Jouy-en-Josas, France

9 (\*) Corresponding authors:

10 `alain.trubuil@inrae.fr`

11 `jean-christophe.palauqui@inrae.fr`

12 `philippe.andrey@inrae.fr`

13

## 14 Abstract

15 Noise plays a major role in cellular processes and in the development of tissues and organs.  
16 Several studies have examined the origin, the integration or the accommodation of noise in  
17 gene expression, cell growth and elaboration of organ shape. By contrast, much less is known  
18 about variability in cell division plane positioning, its origin and links with cell geometry, and  
19 its impact on tissue organization. Taking advantage of the first-stereotyped-then-variable divi-  
20 sion patterns in the embryo of the model plant *Arabidopsis thaliana*, we combined 3D imaging  
21 and quantitative cell shape and cell lineage analysis together with mathematical and computer  
22 modeling to perform a large scale, systematic analysis of variability in division plane orienta-  
23 tion. Our results reveal that, paradoxically, variability in cell division patterns of *Arabidopsis*  
24 embryos is accompanied by a progressive reduction of cell shape heterogeneity. The paradox  
25 is solved by showing that variability operates within a reduced repertoire of possible division  
26 plane orientations that is related to cell geometry. We show that in several domains of the em-  
27 bryo, a recently proposed geometrical division rule recapitulates observed variable patterns,  
28 thus suggesting that variable patterns emerge from deterministic principles operating in a vari-  
29 able geometrical context. Our work highlights the importance of emerging patterns in the plant  
30 embryo under iterated division principles, but also reveal domains where deviations between  
31 rule predictions and experimental observations point to additional regulatory mechanisms.

## 32 1 Introduction

33 In multicellular organisms, cell division is one of the major mechanisms that subtend the elab-  
34 oration and maintenance of functional tissue organizations, as observed for example in animal  
35 epithelia (Lemke and Nelson, 2021). In plants, division is the primary determinant of relative  
36 cell positions because the cellular wall forbids cell displacements and intercalations (Fowler  
37 and Quatrano, 1997). Deciphering the principles that underlie the positioning and orientation  
38 of division plane is thus a central question to understand organ development and morphogen-  
39 esis (Gillies and Cabernard, 2011). The possibility that universal primary physical principles  
40 operate in cleavage plane selection has led to the formulation of several geometrical rules re-  
41 lating division plane positioning to mother cell shape (Minc and Piel, 2012), such as Errera's  
42 rule of plane area minimization for cells dividing symmetrically (i.e., producing daughters of  
43 approximately identical sizes) (Errera, 1888). Though they are essentially phenomenological,  
44 such rules have proved useful as proxys to highlight generic cellular mechanisms that may be  
45 shared between cells with varying morphologies.

46 Stochastic fluctuations, or noise, play a major role in developmental systems (Meyer and  
47 Roeder, 2014; Cortijo and Locke, 2020). For example, at the molecular level, transcriptional  
48 noise has been recognized as a source of heterogeneity in cell fates (Meyer et al., 2017); at  
49 the cellular level, noise in growth rate has been suggested to contribute to the robustness in  
50 the development of organ size and shape (Hong et al., 2016); at higher levels, it has been  
51 proposed that stochastic fluctuations could subtend plant proprioception up to the organ and  
52 organism scales (Moulija et al., 2021). However, in contrast with variability and heterogeneity  
53 in cell and tissue growth, stochasticity in the positioning of the cell division plane has received  
54 much less attention. A noticeable exception is the seminal work of Besson and Dumais, who  
55 showed that in several two-dimensional plant systems with symmetric divisions, a stochastic

56 formulation of Errera's rule accounted better for observed division patterns than its determin-  
57 istic counterpart (Besson and Dumais, 2011). In addition, the impact on tissue organization  
58 of deterministic and variable division rules has been examined from a statistical point of view  
59 (Gibson et al., 2006; Sahlin and Jönsson, 2010; Alim et al., 2012; Wyatt et al., 2015) but  
60 the combinatorics of cell patterns (possible spatial arrangements of cells) that can result from  
61 variable cell divisions has not been examined with a cellular resolution. Overall, systematic  
62 analyses of variability in division plane positioning and of its relations to cell shape and tissue  
63 topological organization are currently lacking.

64 Here, we used the embryo in the model plant *Arabidopsis thaliana* to fill this gap, taking ad-  
65 vantage of the variable cell division patterns observed in this system after initial rounds of  
66 completely stereotyped cell divisions (Mansfield and Briarty, 1991; Capron et al., 2009). We  
67 combined 3D image analysis, cell lineage reconstruction, and computer modeling to systemat-  
68 ically dissect the spatio-temporal diversity of cell shapes and cell divisions and to challenge the  
69 existence of a possible geometrical rule linking cell geometry and division plane positioning.  
70 Paradoxically, our quantifications revealed that cell shapes resulting from variable cell divisions  
71 were evolving within a restrained repertoire of possibilities, highlighting the existence of hidden  
72 geometrical constraints behind the apparent variability of division patterns. We tracked the ori-  
73 gin of these constraints back to the mother cell geometry and show that most of the observed  
74 patterns could be interpreted in light of a recently proposed division rule relating cell shape  
75 and plane positioning (Moukhtar et al., 2019). Our results reveal a unifying principle behind  
76 stereotyped and variable cell divisions in *Arabidopsis* early embryo, suggesting stochasticity  
77 is an emergent property of the evolution of cell shapes during the first generations of cell di-  
78 visions. Cases where observed patterns deviate from the rule illustrate how our model can  
79 highlight domains where, beyond cell geometry, additional regulators may be involved in the  
80 positioning of the division plane.

## 81 2 Results

82 In *Arabidopsis thaliana*, the fourth round of cell division leads to a 16-cell (16C) embryo where  
83 four different domains can be distinguished based on their longitudinal (apical or basal) and  
84 radial (inner or outer) location (Figure 1A). The first four rounds of cell divisions follow invariant  
85 patterns, which can be predicted based on cell geometry (Moukhtar et al., 2019). Hence, 16C  
86 embryos exhibit cell shapes that are specific to each of the four domains (Moukhtar et al.,  
87 2019) and present invariant, symmetrical radial cell organizations in both the apical and the  
88 basal domains (Figure 1BC).

89 Here, we examined whether the stereotypical nature of cell shapes and patterns was main-  
90 tained during late embryo development within each domain. We analyzed cell shapes and cell  
91 patterns over  $\sim 100$  embryos between 1C and 256C stages (rounds 1 to 8 of cell divisions from  
92 the 1C stage). In accordance with previous observations (Yoshida et al., 2014), we initially ob-  
93 served that, from generation 5 onwards, the basal part of the embryo showed little variability in  
94 cell shapes and spatial arrangements, leading to a preserved radial symmetry across domains  
95 and individuals (Figure 1DE). On the contrary, shapes and arrangements of cells were highly  
96 variable in the apical domain. Different orientations and topologies of cell divisions were ob-  
97 served among the different quarters in a given individual as well as among different individuals  
98 (Figure 1DE). This variability resulted in a loss of radial symmetry of cell organization in the

99 apical domain (Figure 1DE). To better characterize and understand the origin of this variability,  
100 we conducted an in-depth quantitative analysis and modeling study of cell shapes and division  
101 patterns.

## 102 2.1 Diversity in cell shape is domain-specific

103 To quantitatively describe cell patterns, we first focused on the diversity of cell shape in the em-  
104 bryo and in its four principal domains defined from the 16C stage (apical/basal  $\times$  inner/outer).  
105 For each embryo, cells were segmented in 3D and their lineage reconstructed back to the  
106 1C stage by recursively merging sister cells (Figure 2A). To allow the classification of cells  
107 into different shape categories, we focused on shape topology rather than on exact geometry  
108 provided by cell segmentation. Shape topology corresponds to the morphological informa-  
109 tion that remains unchanged under position, orientation, scale or other linear and non-linear  
110 geometrical transformations such as anisotropic scaling, shearing, and bending. Distinguish-  
111 ing topology from geometry is important when analyzing the variability of cell patterns since  
112 cells with different geometries can be produced even under invariant orientations of cell divi-  
113 sions. For example, cells in the inner apical domain at the 16C stage can all be described as  
114 tetrahedral pyramids even though none of these cells have the same geometry (Figure 1BC).

115 We introduced a new cell shape topology descriptor based on the cumulative number of di-  
116 vision planes that were positioned through generations to generate a given cell (Figure 2B).  
117 This number, referred to as the number of faces, was automatically computed from cell lin-  
118 eages reconstructed back to the initial 1C stage, which contains two faces (see Material and  
119 Methods). A key advantage of this descriptor is to provide a robust, objective and unambigu-  
120 ous description of cell shape. Contrary to the number of neighboring cells or to the number of  
121 geometrical facets, the number of division faces only depends on the topology of cell divisions  
122 and is insensitive to geometrical fluctuations in the positioning of division planes and to their  
123 curvature.

124 We first applied this descriptor to analyze cell shapes up to the 16C stage (Figure 2C). The  
125 truncated sphere and half-sphere cell shapes of stages 1C and 2C have two and three-face  
126 shapes, respectively. The truncated sphere quarter at 4C has four division faces and is thus  
127 topologically equivalent to a tetrahedron. At stage 8C, the apical cells also have four faces  
128 but a new shape type is observed in the basal domain where cells have five faces, thus being  
129 topologically equivalent to a prism with a triangular basis. At stage 16C, a new cell shape  
130 with six faces was observed, being topologically equivalent to a cuboid. For each of the first  
131 four generations, each embryo domain (one domain from 1C to 4C, two domains at 8C, four  
132 at 16C) contained exactly one cell shape. These results are consistent with the stereotyped  
133 nature of cell division patterns until 16C stage. In addition, our analysis shows that at the whole  
134 embryo scale each generation corresponded to the introduction of a new cell shape with a unit  
135 increase in the number of division faces.

136 Over the next four generations (G5 to G8), we found that more than 99% embryonic cell shapes  
137 were distributed over the three main cell topologies already present at stage 16C, correspond-  
138 ing to shapes with four (3.6%), five (21.9%) and six (73.7%) faces (Figure 2D). From generation  
139 4 onward, cell shapes progressively accumulated in the six-face (cuboid) shape category (Fig-  
140 ure 2E). The systematic unit increase in the number of faces at each generation between G0  
141 and G4 was no longer observed after G4. Hence, the transition between generations 4 and 5  
142 (16C-32C) corresponded to a rupture in the dynamics of embryonic cell shapes.

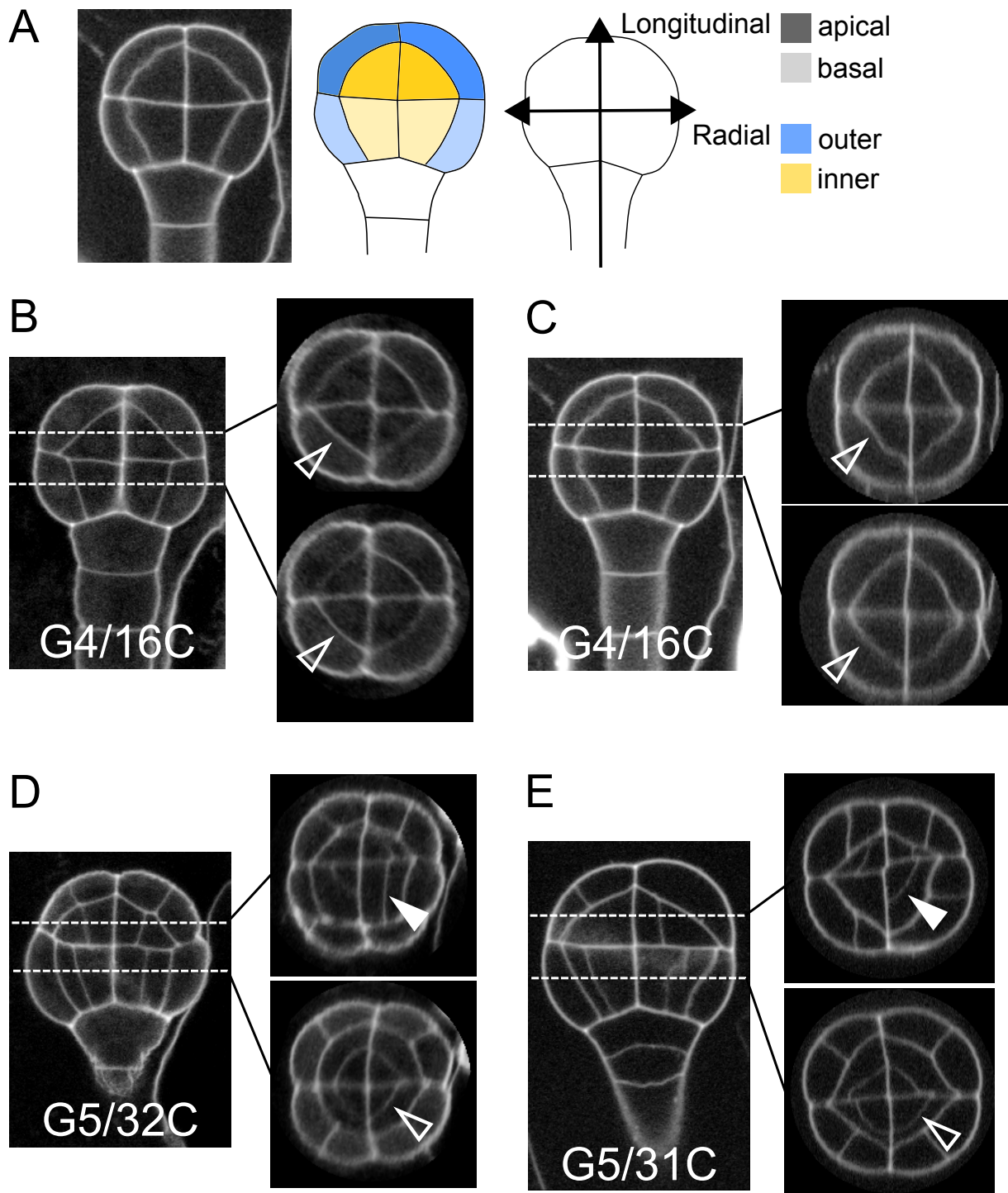


Figure 1: Variability within and between embryos in cell shapes and cell arrangements. (A) The four embryo domains defined by longitudinal and radial axes at stage 16C (longitudinal view): apical/basal  $\times$  outer/inner. (BC) Invariant patterns in embryos up to generation 4 (16C). (DE) Starting from generation 5, embryos show variable cell shapes and cell patterns in the apical domains, both between individuals and between quarters in a given individual. Patterns in the basal domains show little or no variability. Some of the new interfaces at G4 (BC) and at G5 (DE) are labeled using arrow heads (*Empty*: invariant patterns; *Filled*: variable patterns).

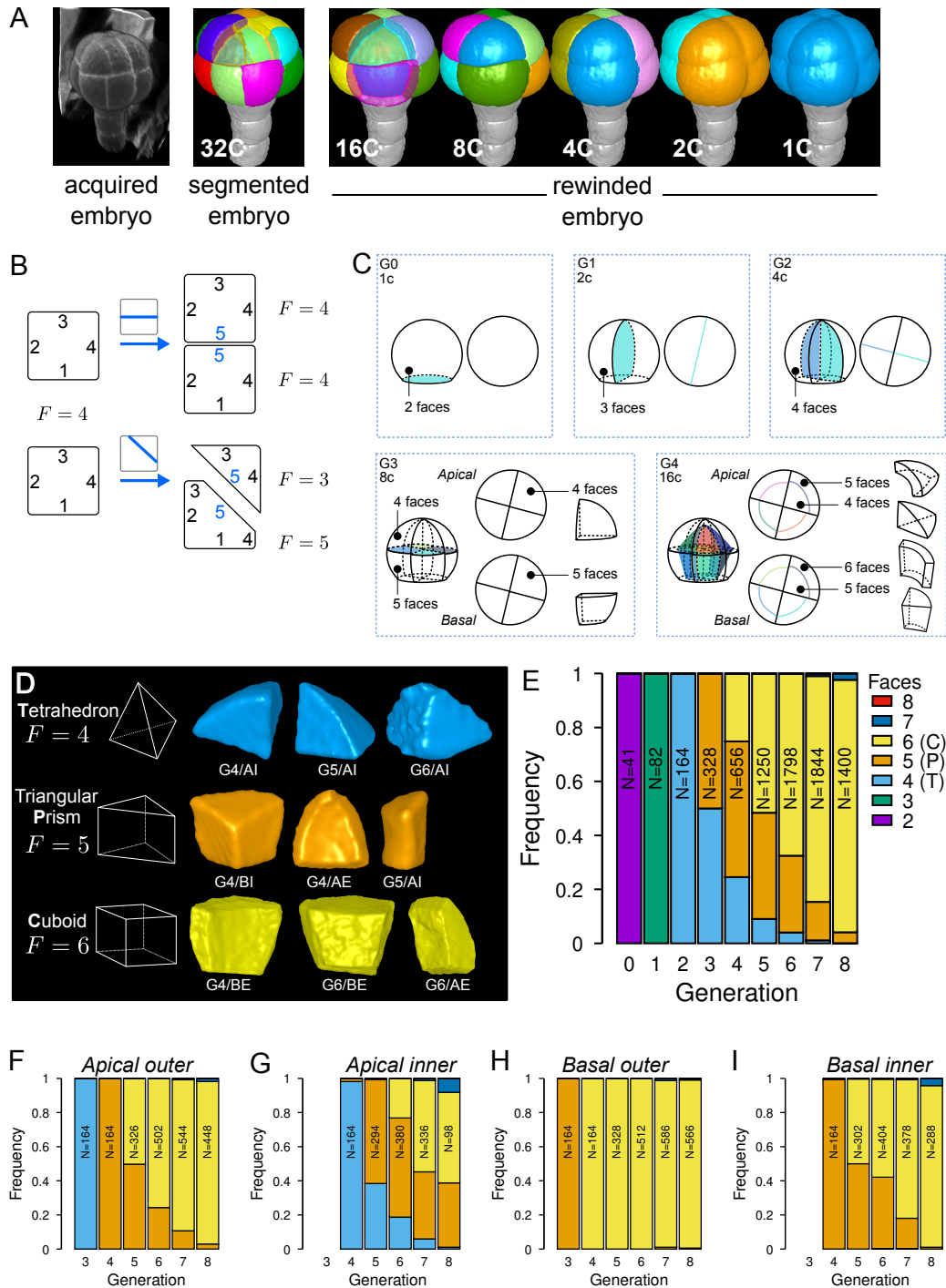


Figure 2: Cell shape diversity in *Arabidopsis thaliana* early embryogenesis. (A) Summary of 3D image analysis pipeline: 3D cell segmentation of confocal image stacks and cell lineage reconstruction by recursive merging of daughter cells. At 32C and 16C stages, some cells are shown transparent to visualize inner cells. (B) Classification of cell shapes based on the number of division interfaces. The scheme illustrates how the number of faces  $F$  may change during a division. In both examples, a cell with initially four faces divides. The number of faces in daughter cells depends on the positioning of the new interface and of whether all original faces are represented in the daughter cells. (C) Shape classification during the first four generations. (D) Samples of the three main classes of cell shapes observed during the late four generations. (E) Proportions of shape classes over the whole embryo during the first eight generations. C: Cuboid; P: Prism; T: Tetrahedron. (F-I) Same as (E) over the outer apical (F), the inner apical (G), the outer basal (H), and the inner basal (I) domain. N: number of observed and reconstructed cells.

143 The evolution of cell shapes at the whole embryo scale masked large differences among the  
144 four domains. Indeed, the domain-specific analysis of cell shapes showed that from generation  
145 4 onward there was almost no variability in the basal outer domain, where all cells remained in  
146 the six-face shape category (Figure 2H). The inner apical domain exhibited the largest variability  
147 in cell shape, with cells having four, five and six-faces observed through several consecutive  
148 generations (Figure 2G). In the basal inner and in the apical outer domains, the diversity was  
149 intermediate, with most cells distributed between the two categories of five and six-face shapes  
150 (Figure 2F and I). The dynamics were also similar in these two domains, with a continuously  
151 increasing proportion of six-face cells.

152 Overall, these results quantitatively confirmed the visual observations that cell patterns in the  
153 apical domain were more variable than in the basal domain. However, our analysis revealed  
154 at the same time a limited range of diversity in cell shapes, with most cell shapes falling within  
155 one out of three main categories. In addition, our data showed that the dynamics of shape  
156 changes during generations 5 to 8 differed from the dynamics observed during generations 1  
157 to 4.

## 158 **2.2 Diversity in division patterns is domain-specific**

159 Since cell shapes are determined by the positioning of division planes, we asked whether the  
160 diversity of cell shapes in the different domains could be related to domain-specific variability in  
161 the positioning and orientation of division planes. We examined this hypothesis by enumerating  
162 observed cell division patterns in each of the four embryo domains. Cell division patterns were  
163 characterized based on the shapes of the mother and of the daughter cells. In addition, we also  
164 took into account the relative orientation of the division planes within the embryo. For example,  
165 a triangular prismatic cell in the outer apical domain can divide according to three orientations  
166 into another prism and a cuboid (Figure 3A). These three possibilities were considered as  
167 distinct division patterns. Using lineage trees, we analyzed and quantified the frequencies of  
168 division patterns during the last four generations, using both observed patterns and patterns  
169 reconstructed at intermediate generations back to the 16C stage. Note that the absence of  
170 embryo bending at these stages ensured that the plane orientation in the embryo at the time  
171 of division could be correctly inferred even for patterns reconstructed from later stages.

172 Starting from the stereotyped cell patterns of 16C embryos, we found three major orientations  
173 of cell divisions in the outer apical domain at the G4-G5 transition (Figure 3B and Figure S3).  
174 Divisions in this domain were systematically anticlinal and oriented parallel to an existing cell  
175 edge, thus separating one vertex from the two other ones at the outer triangular surface of  
176 the cell. The transverse orientation (parallel to the boundary between the apical and basal  
177 domains) was less frequent than the two longitudinal orientations, suggesting a directional  
178 bias in the positioning of the division plane.

179 In the inner apical domain, we also found three main orientations of division planes, all oriented  
180 along the longitudinal axis of the embryo (Figure 3D and Figure S4). Only two of these orien-  
181 tations were parallel to an original vertical face of the cell. Divisions parallel to the horizontal  
182 face of the cells were extremely rare. As in the outer apical domain, these results suggested a  
183 preferential positioning of division planes along a limited number of directions.

184 In contrast with the apical domains, there was only one major orientation of division in each of  
185 the outer and inner basal domains (Figure 3CE). External cells systematically divided accord-

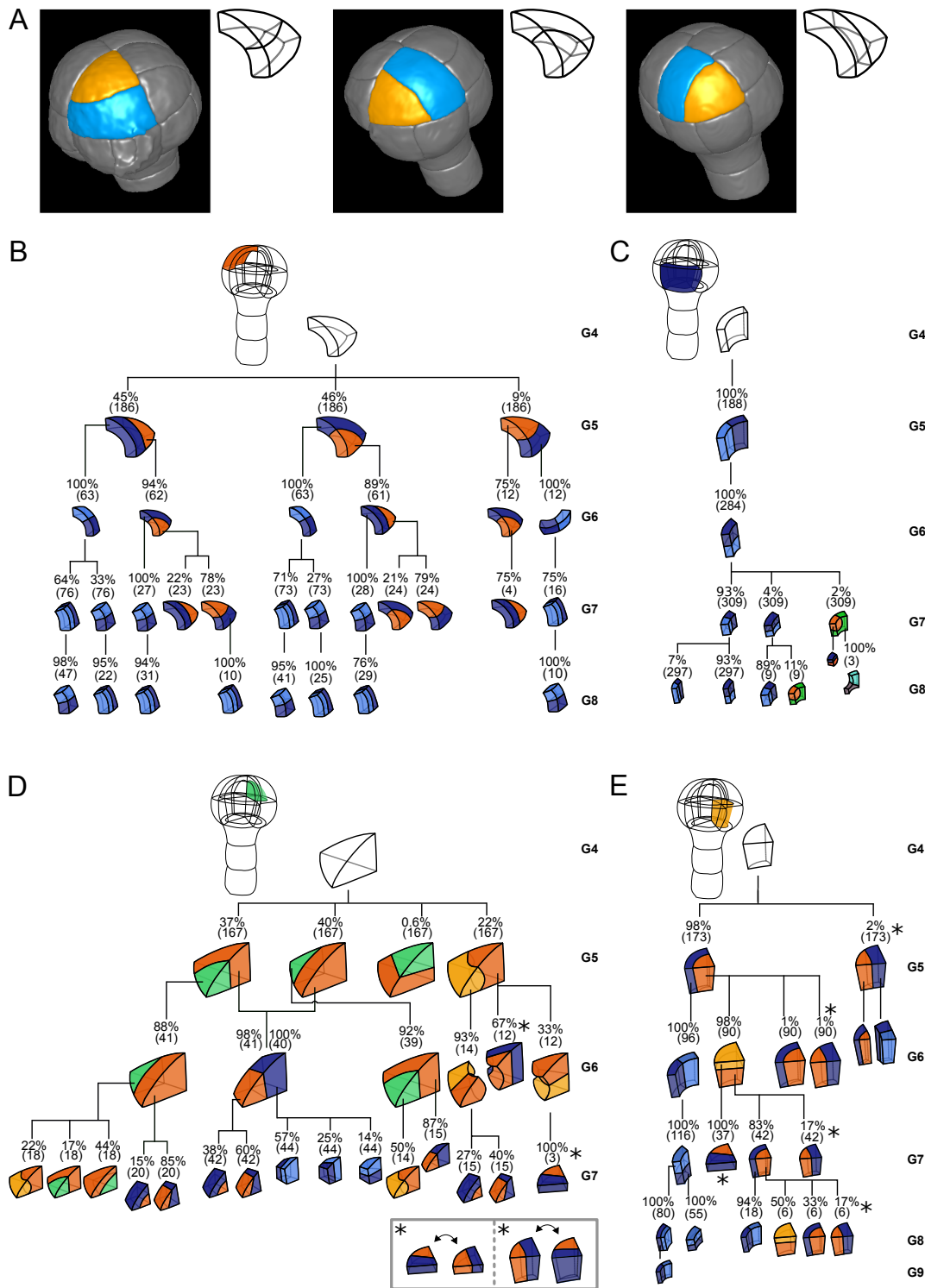


Figure 3: Reconstructed cell lineages in the four embryo domains. (A) Classification of cell division patterns (illustration in the apical outer domain) based on mother and daughter cell shapes and on the absolute orientation of division planes within the embryo. (BCDE) Lineage trees in the apical outer (B), basal outer (C), apical inner (D) and basal inner (E) domains. Each tree shows the observed combinations of cell divisions as a function of cell shapes and of generations. Frequencies were computed based on both observed patterns and patterns reconstructed at intermediate generations when rewinding lineages back to 16C stage from observed configurations. Numbers in parentheses are the total numbers of cases over which the percentages were calculated. Exceptionally rare division patterns are omitted in (B) and (D) for the sake of clarity; complete versions are given in [Figure S3](#) and [Figure S4](#). Asterisks correspond to symmetrical alternatives that were not distinguished in these trees.

186 ing to a longitudinal anticlinal division (intersecting their external face), with a division plane  
187 parallel to the lateral faces of the cell. Internal cells also divided longitudinally but along a  
188 periclinal division (parallel to their external face). This suggests even stronger constraints on  
189 the positioning of division planes within the basal domain compared with the apical domain.

190 The contrast between the apical and the basal domains remained during subsequent genera-  
191 tions, with strongly stereotyped division orientations in the basal domain, except for the division  
192 of the lower cells in the innermost domain at G6 (Figure 3). These results show that variability  
193 in the orientation of division planes was larger in the apical than in the basal domain during the  
194 latest four generations. By comparison with the stereotyped division patterns up to stage 16C,  
195 our analysis further corroborated that the transition between generations 4 and 5 corresponds  
196 to a rupture in the dynamics of division patterns.

## 197 2.3 Division patterns correlate with cell shape topology

198 Since beyond stage 16C the embryo domains differ in the variability of both cell shapes and  
199 division patterns, we hypothesized that this variability could reflect shape-specific division pat-  
200 terns. We addressed this issue by exploiting reconstructed lineage trees to analyze division  
201 patterns in the three main cell shape categories that we identified.

202 Cuboid cells were found in all domains at several generations (Figure 3B–E). These cells  
203 almost exclusively divided into two cuboid daughter cells. Cuboid division resulting in a trian-  
204 gular prismatic daughter cell was only rarely observed. Hence, division of cuboid cells showed  
205 a strong auto-similarity, in that the mother cell shape was almost systematically preserved  
206 through the division. Another remarkable feature of the division of cuboids was spatio-temporal  
207 stationarity, since the division pattern of these cells was the same at all generations and in all  
208 four domains.

209 Cells with a triangular prism topology were also present in the four domains, when rare division  
210 patterns were also considered (Figure 3B–E). These cells showed two division patterns. The  
211 first pattern produced two triangular prisms as daughter cells, through a division parallel to the  
212 triangular faces. The second pattern yielded one triangular prism and one cuboid, through a  
213 division parallel to the quadrilateral faces. Hence, as for cuboid cells, cells with a triangular  
214 prism topology showed auto-similarity in their divisions patterns, even though they could also  
215 generate new cell shapes. In addition, they also showed spatio-temporal stationarity since  
216 their division patterns were similarly observed in all domains and generations where these  
217 cells were present.

218 Cells with a tetrahedral topology were only found in the inner apical domain (Figure 3D). They  
219 also exhibited two division patterns, one producing two triangular prisms and the other produc-  
220 ing one triangular prism and one tetrahedron. Hence, auto-similarity in tetrahedral cells was  
221 not systematic. However, their division patterns were similar throughout successive genera-  
222 tions, showing they were also exhibiting stationarity.

223 Together, these results show that each cell shape exhibited specific division patterns that were  
224 shared among different generations and among different locations within the embryo. The  
225 cuboid shape could be reached from any other cell shape according to the *tetrahedron* →  
226 *triangular prism* → *cuboid* → *cuboid* sequence. Hence, the cuboid shape represented an  
227 absorbing state. In contrast, the tetrahedral shape was the less stable state. These results  
228 explain the decreasing relative frequencies of the tetrahedral and triangular prism cell shapes

229 through generations of cell divisions observed in the four domains (Figure 2E). Because of  
230 shape differences at stage 16C between the four domains, these results may also explain  
231 differences in variability of division patterns. For example, the large variability observed in the  
232 inner apical domain can be interpreted in light of the intermediate triangular prismatic shape  
233 between the tetrahedral and cuboid shapes. Inversely, the absence of shape variability in the  
234 outer basal domain can be related to the absorbing state cuboid shape already present at  
235 G4 in this domain. However, shapes with identical topology were observed in domains with  
236 different variability levels in division orientations, as for example in the outer apical domain and  
237 in the inner basal domain that both have triangular prismatic cells at G4. Hence, other factors  
238 than cell shape topology alone are probably involved in the variability of cell division patterns.

## 239 2.4 Graph theory of cell division reveals variability is constrained

240 To assess whether additional factors govern division patterns beyond cell shape topology,  
241 we asked whether observed division patterns matched predictions from topologically random  
242 divisions. To this end, we used graph theory to describe divisions of polyhedral cells. The  
243 polyhedras (tetrahedron, triangular prism, cuboid) corresponding to the three main cell shapes  
244 observed during generations 5 to 8 can all be represented as planar graphs and displayed  
245 using 2D Schlegel diagrams (Figure 4A) (Grünbaum, 2003). We represented cell divisions as  
246 graph cuts on these polyhedral graphs. A graph cut consists in removing some edges in a  
247 graph so as to partition the original vertices in two disjoint subsets (Greig et al., 1989). Hence,  
248 by removing some edges in the mother cell graph, any cell division resulted in the partitioning  
249 of the  $V$  vertices of the mother cell into two subsets of  $p$  and  $V - p$  vertices. The graphs of the  
250 two daughter cells were obtained by adding new vertices at edge cuts and by introducing new  
251 edges between the added vertices (Figure 4B; Supplementary Information).

252 We used this approach to determine the combinatorial possibilities of division in each of the  
253 three shape topologies. For a given mother cell with  $V$  vertices, we found that any division  
254 separating  $p$  vertices (with  $p \leq V/2$ ) from the  $V - p$  other ones could be fully described based  
255 on  $p$  and the number of mother cell edges that were inherited by the daughter cell inheriting  
256 the  $p$  vertices (Supplementary Information). We further found that in case the inherited edges  
257 formed a cyclic graph, the number of faces in one of the two daughter cells was the same as  
258 in the mother cell and was at most this number in the other daughter cell. In the case of an  
259 acyclic graph, however, at least one daughter would necessarily gain one additional face as  
260 compared with the mother cell (Supplementary Information). This theoretical result explains in  
261 particular why the number of faces in at least one daughter cell necessarily increases when  
262 a tetrahedral cell divides, since the division of tetrahedral cells exclusively corresponds to the  
263 acyclic case. This theory shows why tetrahedral cells cannot be an absorbing state and why  
264 they represent an inevitable source of cell shape diversity through their divisions.

265 For each cell shape topology, we determined all possible combinations of graph cuts under  
266 complete randomness. This allowed us to compute the expected proportions of daughter cells  
267 falling within each cell shape category (Supplementary Information). The theoretical distri-  
268 butions we obtained were significantly different from the observed distributions (Figure 4C),  
269 thus showing observed division patterns were not compatible with the hypothesis of randomly  
270 selected positioning of division planes.

271 Overall, the predictions made using graph theory under unconstrained, random divisions strongly  
272 contrast with observed division patterns, where no or only marginal increases in the number

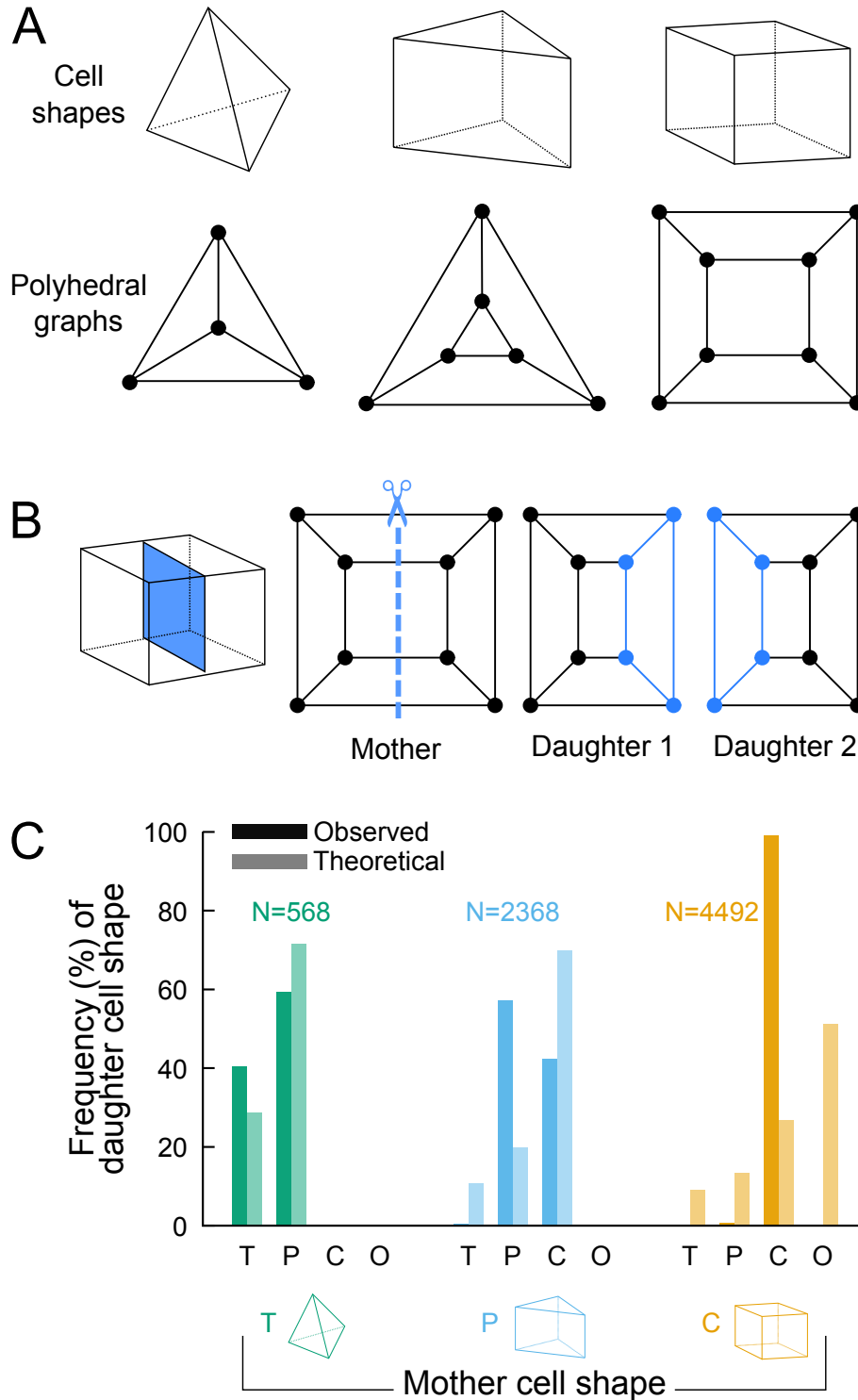


Figure 4: Analyzing cell divisions as graph cuts on polyhedral graphs. (A) The three main cell shapes and their corresponding polyhedral graphs shown as Schlegel diagrams. (B) Cell division as graph cuts: illustration with the division of a cuboid shape. The division shown on the left corresponds to the removal of four edges in the mother cell graph (edges intersected by the dotted line). New vertices and edges added in the graphs of the two resulting daughter cells are shown in blue. (C) Observed and theoretical frequencies of daughter cell shapes during the division of each cell shape. Theoretical predictions were obtained under random graph cuts. *T*: tetrahedron; *P*: triangular prism; *C*: cuboid; *O*: others.

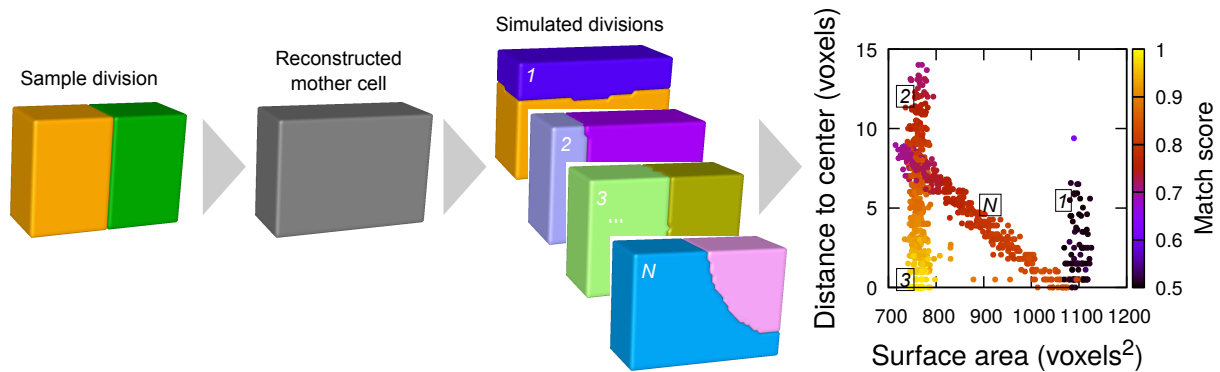


Figure 5: Computational strategy to analyze cell divisions: illustration with a synthetic example (symmetrical vertical division of a cuboid). Starting from a sample division, the mother cell is reconstructed and a large number of divisions at various volume-ratios is simulated. The distance from the cell center and the surface area of the simulated planes are computed. A match score, quantifying the correspondence with the sample division, is computed for each simulated division and represented in pseudo-color. In the present case, the graph shows several families of simulated planes. The location at the bottom left of the distribution of the simulations closest to the sample pattern shows that this division corresponds the minimum plane area among the solutions that pass through the cell center.

273 of faces was observed during the last four generations. Our analysis thus shows that the  
274 observed division patterns are constrained within a limited range of possible combinations.

## 275 2.5 Division planes obey cell geometry constraints

276 To understand the origin of the limited variability in cell division patterns, we asked whether  
277 cell geometry could be sufficient to account for the observed division planes. We previously  
278 showed that, during the first four generations, diverse division patterns (symmetrical as well  
279 as asymmetrical, anticlinal as well as periclinal) could be predicted by a single geometrical  
280 rule according to which planes obey area minimization conditioned on the passing through the  
281 cell center (Moukhtar et al., 2019). The small distance between division plane and cell center  
282 observed during the late four generations (Figure S5) suggested that this rule could also hold  
283 beyond the first four generations. To examine whether this was indeed the case in spite of  
284 diverse division orientations (Figure 3) and volume-ratios (Figure S6), we compared observed  
285 division patterns at G5 to predictions derived from a computational model of cell divisions. We  
286 used a stochastic model that generated binary partitions of a mother cell at arbitrary volume-  
287 ratios, under the constraint of minimizing the interface area between the two daughter cells  
288 (Moukhtar et al., 2019) (see Material and Methods). Several independent simulations with  
289 different volume-ratios were run for each reconstructed mother cell to sample the local minima  
290 of interface area in the space of possible binary partitions.

291 Running the model in synthetic shapes showed that repeating independent simulations at  
292 various volume-ratios generally produced several families of solutions (Figure 5). Each family  
293 corresponded to one of the possible combinations of graph-cuts in the polyhedral graph of the  
294 mother cell. The families could be visualized by plotting the distribution of simulation results  
295 based on surface area and distance to the cell center. For instance, simulations within a  
296 cuboid generated families corresponding to divisions parallel to two of the cuboid faces. In the

297 distribution plots, such families appeared as vertically oriented clusters because of the similar  
298 areas but varying distance to the cuboid center (Figure 5). Other families corresponded to  
299 oblique divisions, isolating one vertex or one edge (Figure 5). These families appeared as  
300 diagonally oriented clusters because area of these solutions increased when the distance to  
301 the center decreased.

302 We scored the similarity between simulation results and observed patterns based on a match-  
303 ing index. This index quantified how well a simulated pattern was reproducing the observed  
304 one based on the overlap between daughter cells in the two patterns (Figure S7 and Material  
305 and Methods). This index ranged between 0.5 (minimal correspondence between simulation  
306 and observation) and 1.0 (perfect correspondence). For a sample division obeying the law of  
307 area minimization constrained by the passing through the cell center, the simulated divisions  
308 that match best the observed pattern should be located at the bottom left of the distribution  
309 plot (Figure 5).

310 We first examined divisions in cells of the outer basal domain, which obey a stereotyped  
311 symmetrical, anticlinal, and longitudinal positioning of the division planes (Figure 3C and Fig-  
312 ure S6). The distribution plots of simulated division planes based on surface area and on  
313 distance to the cell center were reminiscent of those observed in synthetic cuboid shapes  
314 (Figure 6A and Figure S8; compare with Figure 5). Different clusters of simulated planes were  
315 observed, revealing the existence of several local minima of the interface area within the space  
316 of possible partitionings in these cells (Figure 6A). In all analyzed cells, the simulated planes  
317 that matched the observed patterns were systematically found at the bottom left of the distri-  
318 bution plot (Figure 6A and Figure S8), showing that these matching planes were minimizing  
319 the surface area among the solutions that pass close to the cell center. Two other clusters  
320 of simulated planes, corresponding to either oblique or horizontal divisions, poorly matched  
321 observed patterns and had a larger interface area and/or a larger distance to the centroid.  
322 Hence, the anticlinal, highly symmetrical division of the basal outer cells at stage 16C of the  
323 embryo was perfectly predicted by the division rule. In most cells, the matching solutions were  
324 at the bottom of a cluster of solutions displaying a wide range of distances to cell center but  
325 comparable areas, corresponding to a family of parallel longitudinal divisions. This confirmed  
326 our previous result that, by the combined minimization of distance to cell center and of inter-  
327 face area, the rule can predict both the positioning of the division plane and the volume-ratio  
328 of the division (Moukhtar et al., 2019).

329 In the external apical domain, where slightly asymmetrical, non stereotyped divisions were  
330 observed (Figure 3B and Figure S6), we ran the model in reconstructed mother cells that  
331 divided along the three main modes of division observed in this domain. As in the basal  
332 domain, the model generated different families of solutions within each mother cell (Figure 6B-  
333 D), showing the existence of different local minima of surface area for a given cell geometry.  
334 In each case, one of these cluster faithfully matched the observed pattern. The location of this  
335 cluster at the bottom left of the distribution plot suggested that for a given mother cell shape,  
336 the observed division plane could be predicted based on area minimization conditioned on the  
337 passing the through the cell center (Figure 6 and Figure S10, S11 and S12). Remarkably,  
338 simulations belonging to the other, non-matching clusters corresponded to division patterns  
339 observed in other cells (Figure 6B-D). These data can be interpreted as showing the existence  
340 of three principal local minima of surface area in the space of partitionings of each apical  
341 external cell, corresponding to the order 3 rotation invariance of triangular prisms. Our results  
342 also show that cells divide according to the area minimum that fits best with the same division  
343 rule that operates in the outer basal domain.

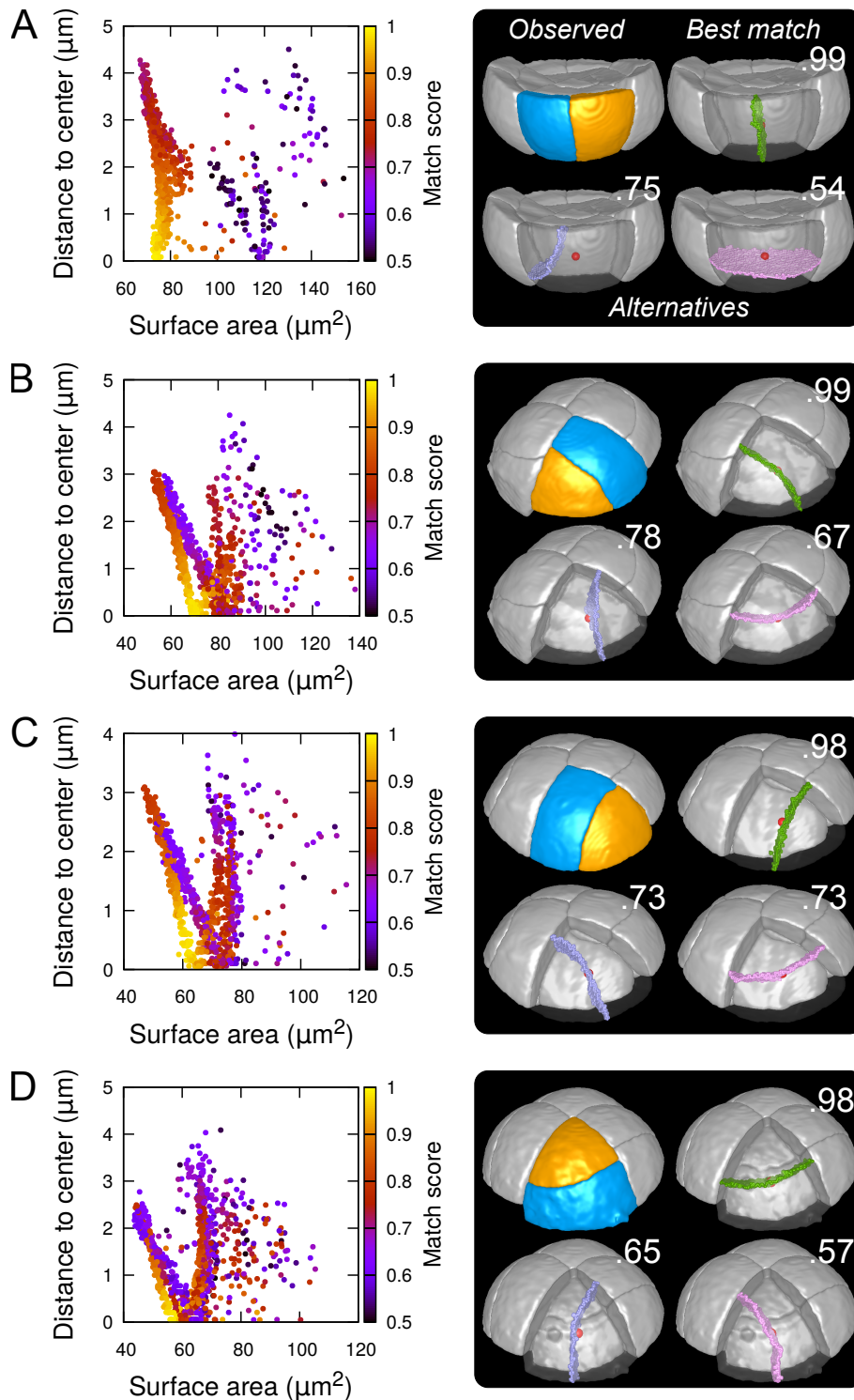


Figure 6: Modeling division patterns at G5 in external cells based on geometrical features. (A) *Left*: distribution plot of simulation results in a basal outer cell (N=1000). Simulated planes are positioned based on their surface area and distance to the mother cell center. The color code indicates the match score between simulated and observed planes. *Right*: observed daughter cells (*Blue* and *Orange*); three simulated planes are shown in the reconstructed mother cell (*Transparent*). *Green*: simulation matching best with observed pattern. *Lavender* and *Pink*: simulations with alternative orientations. Numbers show the corresponding match scores. *Red dot*: mother cell center. (BCD) Same as (A) for three apical outer cells that divided along the three main orientations of division.

344 As in the outer basal domain, simulation results within basal inner cells (were observed divi-  
345 sions were stereotyped, periclinal and strongly asymmetrical; [Figure 3E](#) and [Figure S6](#)) were  
346 distributed among different patterns. However, a key difference with the external domain was  
347 that a few, if any, simulations reproduced the observed divisions ([Figure 7A](#) and [Figure S9](#)).  
348 Since the probability of generating a given interface with the model is inversely related to its  
349 area, the absence or scarcity of reproduced observed patterns suggested that the periclinal  
350 divisions in the inner basal domain did not correspond to the global minimization of interface  
351 area. This was confirmed by the fact that the rare simulations reproducing observed divisions  
352 had generally larger interface areas than alternatives passing as close to the cell center.

353 In the internal apical cells, where experimental variability was the largest ([Figure 3D](#) and [Fig-  
354 ure S6](#)), we found different results depending on the orientation of the division. For cells where  
355 division occurred parallel to an existing interface (yielding a triangular prism and a tetrahe-  
356 dron as daughter cell shapes), we obtained results comparable to those obtained in external  
357 apical cells. Several clusters of simulations were obtained within each cell, and the one re-  
358 producing the actual division was in most cases located at the bottom left of the distribution  
359 ([Figure 7B](#); [Figures S13](#) and [S14](#)). In the other clusters, we observed simulated divisions that  
360 corresponded to patterns observed in other cells ([Figure 7B](#)). Hence, divisions in these cells  
361 were consistent with the existence of multiple local minima of interface area and with the se-  
362 lection, among these, of the minimum that also fits with the minimization of distance to the cell  
363 center. In cells dividing radially (yielding two triangular prisms for daughter cell shapes), some  
364 cells complied with this rule ([Figure 7C](#); [Figure S15](#)) but we also found as many that did not.  
365 In the latter cells, several clusters corresponding to various division orientations were again  
366 observed. However, the cluster reproducing the observed division was either overlapping with  
367 other clusters or was located farther away from the heel of the distribution plot compared with  
368 the alternative clusters ([Figure 7D](#)). This showed that in these cells, the observed division  
369 was not unequivocally corresponding to the minimization of distance to the cell center and of  
370 interface area.

## 371 **2.6 Validation of model predictions**

372 Simulation results obtained with our model suggested that asymmetries in mother cell geome-  
373 try could bias the positioning of the division plane. We evaluated this prediction by examining  
374 the correlation between asymmetries in the mother cell geometry and the division plane ori-  
375 entation. We performed this analysis on the divisions of the 16C apical cells. For these cells,  
376 there was indeed, at the same time, strong self-similarity by rotation of the corresponding  
377 idealized shapes (tetrahedron in the inner part, triangular prism in the outer one) and large  
378 variability in the orientation of the division planes. For each reconstructed mother cell, we  
379 quantified its radial asymmetry by the ratio of left to right extensions and we quantified its rela-  
380 tive longitudinal extension by the ratio of its height to its maximal radial extension ([Figure 8A](#)).

381 For internal apical cells dividing longitudinally with a triangular prismatic daughter cell on the  
382 left, the left extension was on average smaller than the right extension ([Figure 8B](#), *Green*). The  
383 reverse was observed for the internal cells that divided with a triangular prismatic daughter  
384 located on the right ([Figure 8B](#), *Yellow*). For the internal cells that divided horizontally or  
385 longitudinally with no left/right asymmetry in plane positioning, there was no pronounced radial  
386 asymmetry ([Figure 8B](#), *White* and *Pink*) but, compared with cells that divided longitudinally,  
387 they exhibited a larger longitudinal extension ([Figure 8C](#)). Hence, in internal apical cells, the

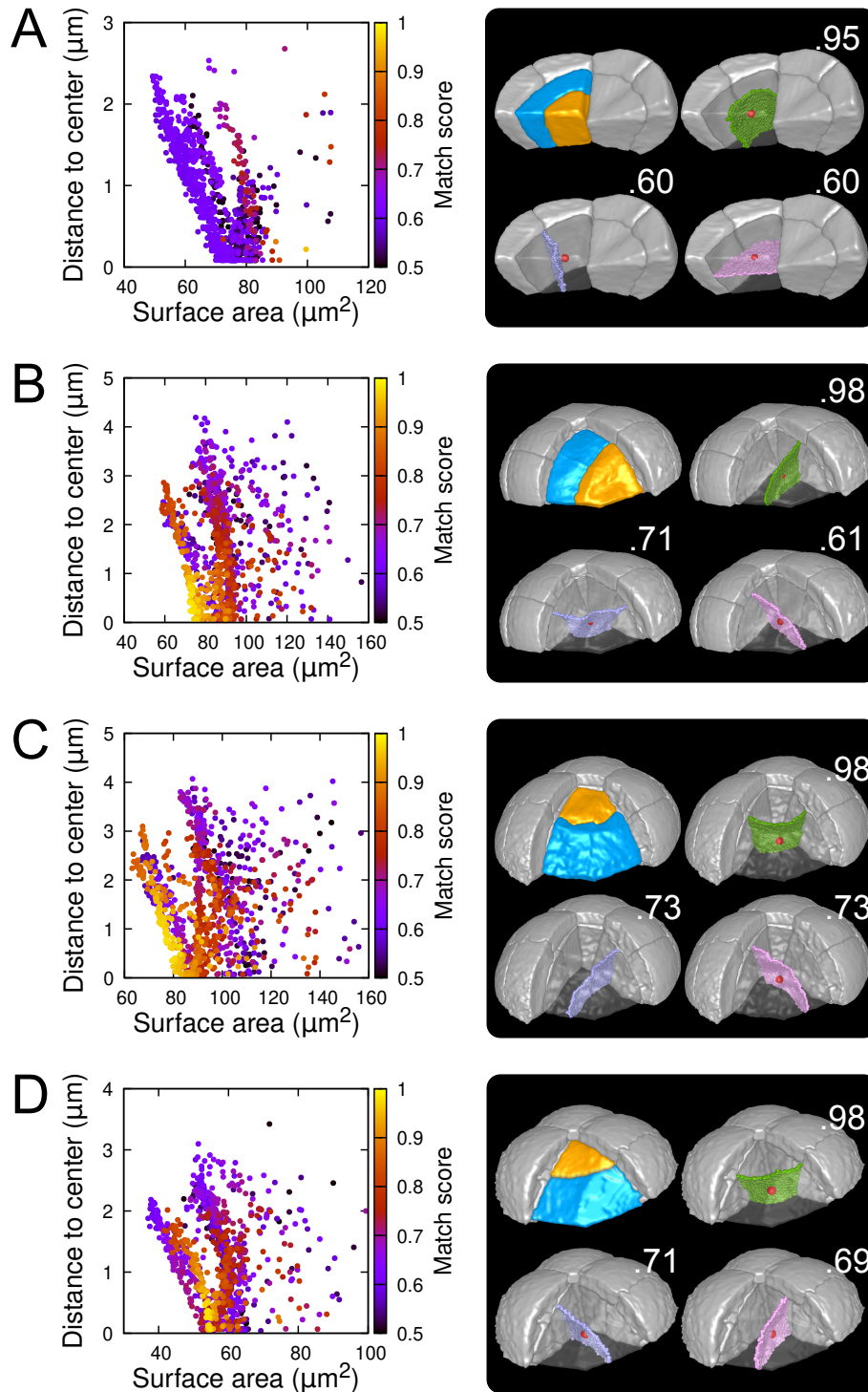


Figure 7: Modeling division patterns at G5 in internal cells based on geometrical features. (A) *Left*: distribution plot of simulation results in a basal inner cell (N=1000). Simulated planes are positioned based on their surface area and distance to the mother cell center. The color code indicates the match score between simulated and observed planes. *Right*: observed daughter cells (*Blue* and *Orange*); three simulated planes are shown in the reconstructed mother cell (*Transparent*). *Green*: simulation matching best with observed pattern. *Lavender* and *Pink*: simulations with alternative orientations. Numbers show the corresponding match scores. *Red dot*: mother cell center. (BCD) Same as (A) for three apical inner cells.

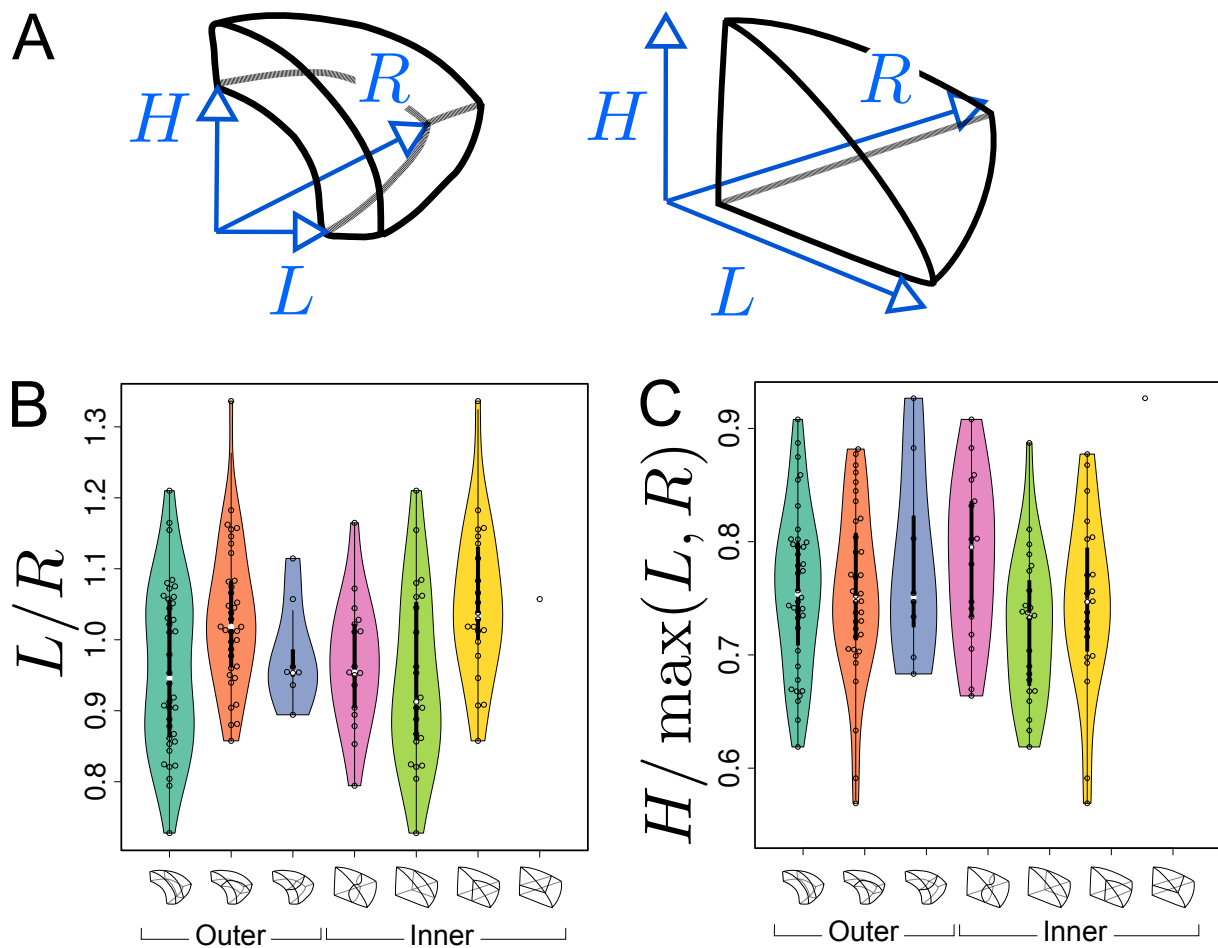


Figure 8: Asymmetries in mother cell geometry in the apical domain at stage 16C and their relations with division plane orientation. (A) Measured extensions of outer (*Left*) and inner (*Right*) mother cells. (B) Radial asymmetry. (C) Relative longitudinal extension. Measurements were performed on mother cells reconstructed at G4/16C from observed embryos at G5 or G6.

388 position of the division plane matched the geometrical asymmetry of the mother cell along  
389 different directions.

390 Similar trends were observed in the outer apical cells. Among these, cells dividing longitudi-  
391 nally with a cuboid daughter cell located on the left had on average a smaller left than right  
392 extension (**Figure 8B**, *Turquoise*). The reverse was observed for the cells that divided with a  
393 cuboid daughter cell located on the right (**Figure 8**, *Orange*). As in the inner domain, the radial  
394 asymmetry was less pronounced for the outer apical cells that divided horizontally (**Figure 8B**,  
395 *Blue*). Compared with the inner domain, however, it was less clear whether their longitudinal  
396 extension was larger than in cells dividing longitudinally (**Figure 8C**), which may be due to the  
397 limited number of cells that were observed to divide horizontally.

398 Overall, these results show that apical cells at 16C presented directional asymmetries and that  
399 division planes tended to be oriented parallel to the smallest extension. This suggests that the  
400 diversity of division plane orientations for a given shape topology reflects geometrical diversity,  
401 in accordance with the predictions from our geometrical division rule.

## 402 **2.7 Attractor patterns buffer variability of cell division orientation**

403 The above results show that from one generation to the next, there is large variability in cell  
404 division orientation in some embryo domains. Across several generations, the combinatorial  
405 possibilities between different orientations can potentially lead to a large number of distinct cell  
406 patterns. To determine whether this was indeed the case, we analyzed division patterns over  
407 two consecutive generations.

408 In the outer apical domain, three main orientations of cell divisions were observed at G5.  
409 Variability in division orientation was less pronounced in the subsequent generations, which  
410 presented alternation of division plane orientations (**Figure 3B**). As a result, similar cell pat-  
411 terns could be reached at generation 6 through different sequences of division events from G4  
412 (**Figure 9A**).

413 In the protodermal layer of the basal domain, some variability was first observed at the transi-  
414 tion between G6 and G7, where in 16 out of 303 cases (5.3%) the division plane was oriented  
415 transversely instead of longitudinally (**Figure 3C**). Similarly, some cells (19/297, 6.4%) at G7  
416 divided longitudinally instead of transversely (**Figure 3C** and **Figure 9C**). Some cells in early  
417 heart stage embryos of our collection had already undergone an additional round of cell di-  
418 vision, allowing to examine the evolution of such patterns. We observed that the cells that  
419 had exceptionally divided longitudinally at G7 led to daughters cells that divided transversely  
420 at the next generation, thus restoring at G9 the same  $2 \times 2$  checkerboard cell pattern than ob-  
421 tained along the transverse then longitudinal path followed in most embryos from G7 to G9  
422 (**Figure 9C**).

423 In the inner basal domain, cell divisions were strongly stereotyped, following periclinal patterns  
424 that yield the precursors of the future vascular tissues (**Figure 3E** and **Figure 9B**, *Left*). At G5,  
425 however, 3 out of 153 cases (2%) in our dataset showed an anticlinal pattern (**Figure 3E** and  
426 **Figure 9B**, *Right*). One of these cases was reconstructed from an embryo acquired at G6.  
427 This allowed to observe that one of the two daughter cells of the anticlinal division at G5 had  
428 divided periclinally at G6, thus restoring the formation of a new cell layer as in the standard  
429 case (**Figure 9B**). This suggests that, in the inner basal domain also, similar cell patterns can  
430 be reached through different paths in spite of variability in division plane positioning.

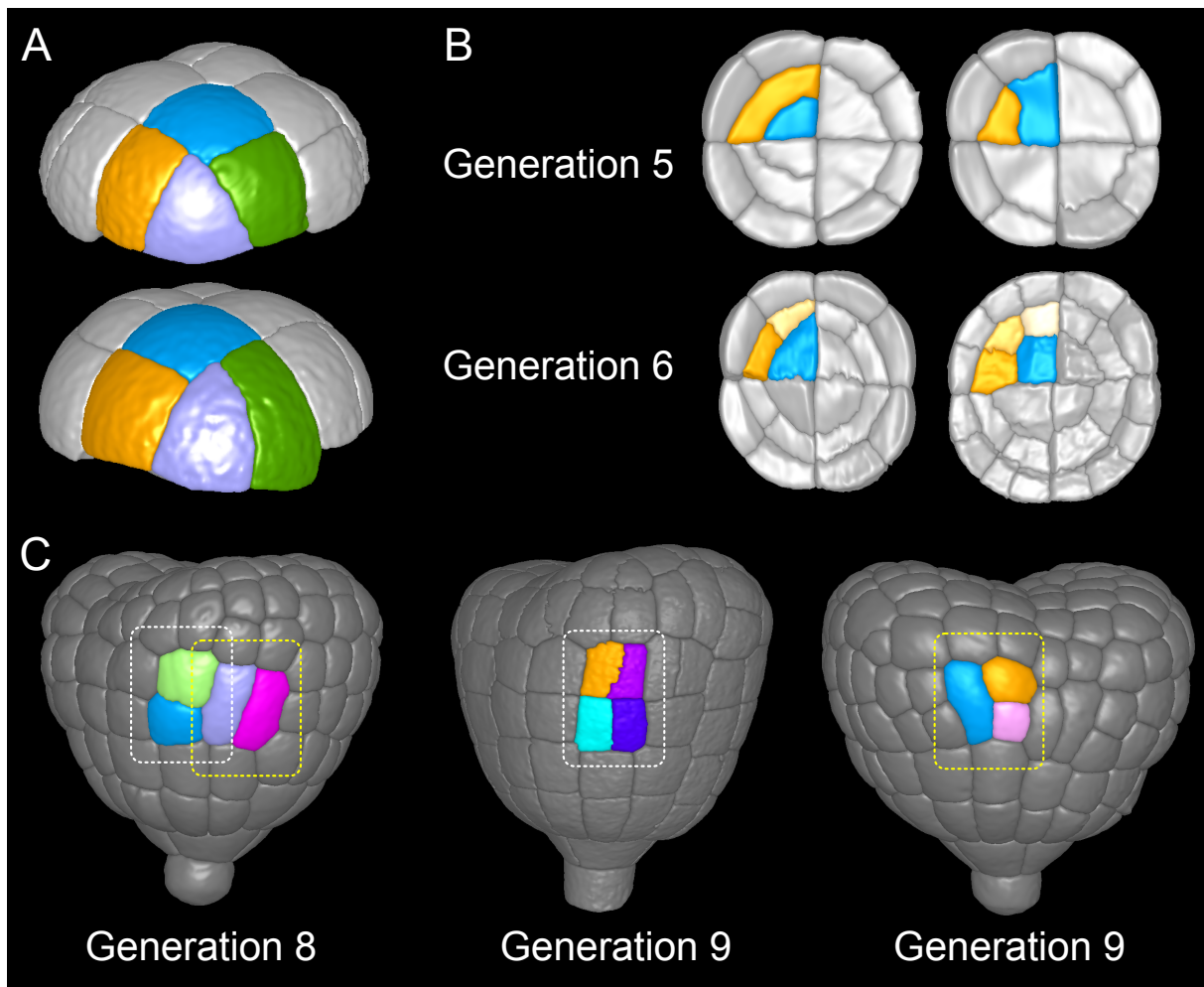


Figure 9: Attractor patterns buffer variability in division plane positioning. (A) Similar cell patterns observed at G6 in the apical outer domain that have been reached through distinct cell division paths from G4. (B) Main (*Left*) and rare (*Right*) division patterns in the inner basal domain at G5 and corresponding patterns at G6. (C) Main (*White box*) and rare (*Yellow*) patterns observed at G8 and G9 in the outer basal domain.

431 These results show the existence of invariant cell patterns that can be reached through differ-  
432 ent paths of successive cell divisions from stage 16C. This suggests that a significant part of  
433 the variability in cell division positioning observed during the late four generations of embryo-  
434 genesis is buffered when considering time scales that span several generations, thus ensuring  
435 the construction of robust cell organizations in spite of local spatio-temporal variability.

### 436 3 Discussion

437 Previous attempts to decipher the principles that underlie the position and orientation of di-  
438 vision planes have been focused on geometrical rules predicting the division plane position  
439 relatively to the mother cell geometry, and on their impact on global tissue organization and  
440 growth. Much less attention has been given to the prediction of tissue organization with a ge-  
441 ometrical precision at the individual cell level. The *Arabidopsis* embryo is a remarkable model  
442 to address the existence and nature of geometrical division rules, as it presents invariant di-  
443 vision patterns during the first four generations followed by intra- and inter-individual variable  
444 patterns for the next four generations. Here, we provided a detailed quantitative analysis of  
445 this variability and used theoretical and computational modeling of cell divisions to investigate  
446 its origin. We show that strong regularities are hidden behind the apparent variability and that  
447 most of the observed patterns can be explained by a deterministic division rule applied in a  
448 geometrical context affected by the stochasticity of the precise positioning of division plane.

449 Deterministic cell division patterns have been interpreted in light of geometrical rules linking  
450 cell shape to division plane (Minc and Piel, 2012). The shortest path rule, according to which  
451 cells divide symmetrically so as to minimize the interface area between daughter cells (Errera,  
452 1888), has been shown to operate in several plant tissues such as fern protonema (Cooke  
453 and Paolillo Jr, 1980), algae thallus (Dupuy et al., 2010), *Arabidopsis* meristem (Sahlin and  
454 Jönsson, 2010) or early embryo (Yoshida et al., 2014; Moukhtar et al., 2019). However, it was  
455 also shown that stochastic rules are required to account for division patterns in many tissues  
456 with 2D geometries (Besson and Dumais, 2011). Hence, a stochastic division principle would  
457 a priori be the most likely candidate interpretation of the variable division patterns we reported  
458 here in late *Arabidopsis* embryo. Our results actually point to a different interpretation for  
459 this variability. Indeed, for a given cell geometry, the observed plane orientation and position  
460 matched in most cases the global optimum according to the rule of area minimization condi-  
461 tioned on the passing through the cell center, and we could correlate the plane orientation with  
462 asymmetries in directional cell extensions.

463 Based on these results, we propose that variability in cell division patterns could originate from  
464 fluctuations in mother cell geometry rather than from the division rule. The tetrahedral and  
465 triangular prismatic shape topologies of apical cells at stage 16C are rotationally symmetric. If  
466 cells were perfectly symmetric, the various plane orientations (4 in inner apical cell, 3 in outer  
467 apical cells) would be equally probable according to the geometrical rule. We hypothesize that  
468 actual geometrical deviations from perfect symmetry suppress this equi-probability and induce  
469 a single global minimum, which would be selected during the division. Accordingly, variability  
470 in division plane orientations in the apical domain would not ensue from a stochastic division  
471 rule, but rather from a deterministic principle expressed within a varying mother cell geometry.  
472 Note, however, that our sample sizes do not allow to definitively rule out a possible stochastic  
473 selection of division plane orientation, in particular in light of the results obtained in the inner

474 apical domain with cells dividing longitudinally. Further studies will be required to definitively  
475 distinguish between these two hypotheses and to further dissect the respective contributions  
476 of intrinsic (variability of plane positioning for a given cell geometry) and of extrinsic (variability  
477 due to fluctuations in mother cell geometry) noise in the selection of the division plane.

478 Our data reveal an abrupt change in the dynamics of cell shapes and cell division patterns at  
479 the transition between generations 4 (16C) and 5 (32C). Up to generation 4, division patterns  
480 were stereotyped and each generation corresponded to the introduction of a new cell shape  
481 with a unit increase in the number of cell faces. In contrast, we observed from generation  
482 5 onward a strong variability in division patterns with a concomitant reduction in cell shape  
483 variability, as cell shapes progressively converged towards a single 6-face shape topology.  
484 Graph cut theory on polyhedral graphs together with our hypothesis of a deterministic division  
485 principle operating in a stochastic cell geometry offer a parsimonious interpretation of this  
486 apparent paradox. On the one hand, our theory shows that the division of the tetrahedral  
487 cells from generation 2 inevitably generates novelty with one obligatory prismatic daughter  
488 cell shape. We also show that triangular prismatic shapes that appear at generation 3 are  
489 theoretically twice less self-reproducible than the cuboid shapes that appear for the first time  
490 at generation 4. Beyond this stage, cell division through the cell center and area minimization  
491 tend to preserve the cuboid shape of the mother cell in the two resulting daughters. On the  
492 other hand, variability in division patterns emerges at generation 5 because of the almost,  
493 but not exactly, rotation-symmetrical cell geometries reached for the first time at stage 16C.  
494 Hence, our study reveals that a common underlying geometrical rule can account for cell  
495 division patterns with radically different traits.

496 Our interpretation of the variability in division orientations raises the issue of the origin of vari-  
497 ability in cell geometry within a given cell shape category. In spite of genetic controls, any  
498 given division pattern is subject to random fluctuations that affect the precise positioning of the  
499 cleavage planes (Schaefer et al., 2017). This noise in the positioning of division planes ac-  
500 cumulate through embryo generations, resulting in non-perfectly symmetrical shapes at stage  
501 16C. A modeling study previously reported the importance of stochastic positioning of cleavage  
502 planes at the 2C-4C transition in the patterning of vascular tissues (De Rybel et al., 2014). In  
503 our case, it is likely that errors accumulated over the 2C-4C and 4C-8C transitions contribute to  
504 the geometrical asymmetries that bias division plane positioning at the 16C-32C stage. Hence,  
505 our results strongly suggest that not only genetic patterning (De Rybel et al., 2014) but also  
506 division patterning could be influenced by the geometric memory of past stochastic events.

507 Several studies have highlighted the importance of noise and stochastic processes in plant  
508 developmental programs (Korn, 1969; Meyer and Roeder, 2014; Hong et al., 2018). At the  
509 cellular level, these processes have been described essentially for cell growth. For example,  
510 heterogeneity in cell growth patterns was shown essential for the robustness of organ shapes  
511 (Hong et al., 2016). It is yet unclear, however, whether variability in division orientation has  
512 functional implications, be it in the mechanical shaping of the embryo or in the establishment  
513 of growth gradients that would subtend the future evolution of the embryonic shape. Import-  
514 antly, homeostatic mechanisms compensating for cell growth variability have been described.  
515 For example, at the cellular level, larger relative growth rates in smaller cells (Willis et al., 2016)  
516 or DNA-dependent dosage of a cell cycle inhibitor (D'Ario et al., 2021) have been proposed  
517 to subtend cell size homeostasis in the shoot apical meristem; at the tissue level, mechanical  
518 feedbacks have been described that buffer growth heterogeneities between cells (Hervieux  
519 et al., 2017). We reveal here in several embryo domains the existence of attractors in embryo  
520 cell patterns that can be reached through different division sequences, thus generalizing past

521 observations in the root embryonic axis (Scheres et al., 1995). As for cell growth patterns,  
522 these attractor patterns can be interpreted as buffering heterogeneity in division plane orien-  
523 tation. Hence, our results reveal a new compensation mechanism at the cellular level that, in  
524 addition to known cell growth regulations, could operate in developing plant tissues to generate  
525 robust supra-cellular patterns.

526 Previous studies have modeled the topology of divisions in 2D. It was shown for example  
527 how an average of 6 neighbors per cell could emerge from random symmetrical divisions  
528 (Graustein, 1931; Gibson et al., 2006). Based on Markov chain modeling, it was also shown  
529 how steady-state distributions in the number of faces or of neighbors could be computed in pro-  
530 liferating epithelia (Gibson et al., 2006; Cowan and Morris, 1988). The topology of a 2D division  
531 in a polygonal shape can simply be modeled as a combinatorial choice of two polygonal edges  
532 (Cowan and Morris, 1988; Gibson et al., 2006). Unfortunately, this approach cannot be gener-  
533 alized to polyhedral cells in three dimensions. Here, we proposed a solution to this problem by  
534 modeling the topology of division in polyhedral cells as cuts on polyhedral graphs. The large  
535 differences between predicted daughter shape distributions under topologically random divi-  
536 sions of mother cells and observed distributions revealed the existence of strong constraints  
537 on division plane positioning at the 16C-32C transition. Though this is probably challenging,  
538 it would be of further interest to explore the potential of the proposed graph theoretical ap-  
539 proach to address the existence of, and to theoretically derive, the asymptotic distributions  
540 of 3D shapes under random or more elaborate topological rules, as was done in 2D tissues  
541 (Cowan and Morris, 1988; Gibson et al., 2006).

542 The results of the present study show that the same geometrical rule that accounted for cell  
543 division patterns during the first four generations is also consistent with the positioning of di-  
544 vision planes beyond the dermatogen stage. However, we found contrasting results among  
545 different embryo domains and, to a lesser extent, among different orientations of division. In  
546 the protodermal domains of both the upper and the lower domains, both the volume-ratios and  
547 the positioning of the cleavage interface could be accurately predicted following the geomet-  
548 rical rule. In contrast, divisions markedly departed from the rule in the lower inner domain.  
549 An intermediate situation was observed in the inner apical domain, where the rule accounted  
550 for all but the longitudinal radial orientation. Auxin signaling has been suggested as required  
551 for cells to escape the default regime of division plane minimization and to control periclinal  
552 divisions at the previous (8C-16C) generation of cell divisions (Yoshida et al., 2014), which  
553 could involve a modulation of cell geometry by auxin signaling (Vaddepalli et al., 2021). At  
554 subsequent generations, it has instead been reported that the first vascular and ground tissue  
555 cells divided periclinally along their maximal (longitudinal) extension when the auxin response  
556 was impaired by a ARF5/MP mutation or local ARF inhibition (Möller et al., 2017). In the shoot  
557 apical meristem, cells preferentially divide longitudinally at the boundaries of emerging organs,  
558 where auxin responses are low (Louveau et al., 2016). Hence, it is unclear whether specific  
559 auxin responses are involved in the longitudinal divisions observed in the inner domains. Me-  
560 chanical forces have been shown to alter division plane orientations in in vitro-grown cells  
561 (Lintilhac and Vesecky, 1984), and it was shown in the shoot apical meristem that tissue me-  
562 chanical stress could override cell geometry in the specification of plane positioning (Louveau  
563 et al., 2016). It was also recently found that the orientation of cell division during lateral root  
564 initiation correlated with cellular growth (Schütz et al., 2021). Hence, one can speculate that  
565 the differences in cell environments between the inner and the outer embryo domains may in-  
566 duce different mechanical contexts with differential impacts on the determination of the division  
567 plane orientation.

## 4 Material and methods

### 4.1 Sample preparation and image acquisition

*mPS-PI staining.* *Arabidopsis* siliques were opened and fixed in 50% methanol and 10% acetic acid five days at 4°C. Samples were rehydrated (ethanol 50%, 30%, 10% and water) then transferred 3 hours in a 0.1 N NaOH 1% SDS solution at room temperature. Next, samples were incubated 1 hour in 0.2 mg/ml  $\alpha$ -amylase (Sigma A4551) at 37°C and bleached in 1.25% active  $\text{Cl}^-$  30 to 60 seconds. Samples were incubated in 1% periodic acid at room temperature for 30 min and colored by Schiff reagent with propidium iodide (100 mM sodium metabisulphite and 0.15 N HCl; propidium iodide to a final concentration of 100 mg/mL was freshly added) overnight and cleared in a chloral hydrate solution (4 g chloral hydrate, 1 mL glycerol, and 2 mL water) few hours. Finally, samples were mounted between slide and cover slip in Hoyer's solution (30 g gum arabic, 200 g chloral hydrate, 20 g glycerol, and 50 mL water) using spacers.

*Confocal microscopy and image acquisition.* Acquisitions were done with a Zeiss LSM 710 confocal microscope as described previously (Truernit et al., 2008). Fluorescence signals were recorded using a 40x objective and digitized as 8-bit 3D image stacks with a near-to-optimal voxel size of  $0.17 \times 0.17 \times 0.35 \mu\text{m}^3$ .

### 4.2 Image processing and analysis

Noise in acquired 3D images was attenuated by applying Gaussian smoothing (with parameter  $\sigma = 0.5$ ) under the Fiji software (Schindelin et al., 2012). Cells were segmented by applying the 3D watershed transform (Vincent and Soille, 1991) to images after non-significant minima had been removed using minima imposition (Soille, 2003). The two operations were performed using the Morphological Segmentation tool of the MorphoLibJ suite (Legland et al., 2016). All segmentations were visually checked and a modified version of the MorphoLibJ plugin was developed to correct over- and under-segmentation errors, if any, based on the interactive modification of watershed initialization seeds.

The cell lineages were manually back tracked, processing embryos from the younger to the older ones (using the number of cells as a proxy for developmental stage). Based on the cellular geometries and organizations, sister cells were paired so as to minimize wall discontinuities in reconstructed mother cells. Lineage reconstruction was performed using TreeJ, an in-house developed Fiji plugin. Reconstructed cell lineage trees were exported as Ascii text files for further quantitative analysis.

Segmented images and lineages trees were processed under Matlab (MATLAB, 2012) to localize cells within the embryo and to assign them to embryo domains (inner or outer, apical or basal). Cell volumes were obtained by multiplying the number of voxels of each cell by unit voxel volume (product of spatial calibration in XYZ directions). Mother cells were reconstructed by merging the segmentation masks of daughter cells. For each division, volume-ratio was computed as the ratio between the smaller cell volume and the mother cell volume. Three-dimensional triangular meshes of segmented cells and of their interfaces with neighbour cells were computed under AvizoFire (©2013 Visualization Sciences Group, an FEI Company). The cell interface meshes were processed by a python script to automatically measure ratios of cell extensions along different directions. To this end, we first computed the intersection lines

609 between side meshes by determining their shared vertices. Then, vertices at intersections be-  
610 tween three connected intersection lines were identified as cell corners. Cell extensions were  
611 obtained as Euclidean distances between corner vertices.

612 The number of faces per cell was computed using cell lineage trees with a python script.  
613 Mother cells were reconstructed up to the first embryonic cell by recursively merging sister  
614 cells. During this process, the generation at which each division plane had been formed was  
615 recorded. This allowed to determine for each observed cell the number of different genera-  
616 tions at which interfaces with neighboring cells had been created. This number was taken as  
617 the number of faces for the cell. For the first embryonic cell, there were two interfaces, one  
618 corresponding to the wall separating this cell from the suspensor and the other corresponding  
619 to the separation with the outside of the embryo.

### 620 4.3 Computer modeling of cell divisions

621 **Computer simulations.** Cell divisions in reconstructed mother cells were simulated using the  
622 model we introduced previously (Moukhtar et al., 2019). For each simulation, the volume-ratio  
623  $\rho$  of the division (volume of the smaller daughter cell to the volume of the mother) was randomly  
624 drawn between 0.2 and 0.5. Each voxel of the mother cell mask was initially assigned to one  
625 or another of the two daughter cells with probability  $\rho$  and  $1 - \rho$ , respectively. The Metropolis  
626 algorithm (Metropolis et al., 1953) was then used to iteratively minimize the interface area  
627 between the two daughter cells. The algorithm iterated 5000 cycles of  $N$  steps each,  $N$  being  
628 the number of voxels in the binary mask of the mother cell. At each step, a voxel was randomly  
629 chosen. Its assignment to one or the other of the two daughter cells was flipped if this induced a  
630 decrease in the interface area. Otherwise, the flip was accepted with probability  $\exp(-\beta\Delta A)$ ,  
631 where  $\Delta A$  represented the change in interface area induced by the flip. The parameter  $\beta$   
632 was automatically adjusted at the end of each cycle so that about 5%, on average, of the  
633 candidate flips that would increase interface area were accepted. For each mother cell, 1000  
634 independent simulations were run.

**Scoring simulated divisions.** The similarity between the simulated and observed divisions  
was scored based on their spatial overlap (Figure S7). Let  $A$  and  $B$  denote the sets of voxels  
in the two daughter cells of an observed division, and let  $A'$  and  $B'$  denote the two sets in a  
simulated division. The score quantifying the match between the two partitions of the mother  
cell space was defined as:

$$\text{score} = \max \left\{ \frac{|A \cap A'| + |B \cap B'|}{|A \cup B|}, \frac{|A \cap B'| + |B \cap A'|}{|A \cup B|} \right\}$$

635 This score varied between 0.5 (the minimum possible overlap) and 1.0 (perfect overlap).

## 636 Acknowledgments

637 This work was supported by the MIA and BAP departments of INRA (funding support to EL)  
638 and has benefited from the support of IJPB's Plant Observatory technological platforms. We  
639 thank Herman Höfte for his comments and feedback on a first version of our manuscript. The  
640 IJPB benefits from the support of Saclay Plant Sciences-SPS (ANR-17-EUR-0007).

## References

- 641
- 642 Alim, K., Hamant, O., and Boudaoud, A. (2012). Regulatory role of cell division rules on tissue  
643 growth heterogeneity. *Frontiers in Plant Science*, 3:174.
- 644 Besson, S. and Dumais, J. (2011). Universal rule for the symmetric division of plant cells.  
645 *Proceedings of the National Academy of Sciences of the United States of America*,  
646 108(15):6294–6299.
- 647 Capron, A., Chatfield, S., Provart, N., and Berleth, T. (2009). Embryogenesis: pattern forma-  
648 tion from a single cell. *The Arabidopsis Book*, 7:e0126.
- 649 Cooke, T. J. and Paolillo Jr, D. J. (1980). The control of the orientation of cell divisions in fern  
650 gametophytes. *American Journal of Botany*, 67(9):1320–1333.
- 651 Cortijo, S. and Locke, J. C. W. (2020). Does gene expression noise play a functional role in  
652 plants? *Trends in Plant Science*, 25:1041–1051.
- 653 Cowan, R. and Morris, V. B. (1988). Division rules for polygonal cells. *Journal of Theoretical*  
654 *Biology*, 131:33–42.
- 655 D’Ario, M., Tavares, R., Schiessl, K., Desvoyes, B., Gutierrez, C., Howard, M., and Sablowski,  
656 R. (2021). Cell size controlled in plants using DNA content as an internal scale. *Science*,  
657 372:1176–1181.
- 658 De Rybel, B., Adibi, M., Breda, A. S., Wendrich, J. R., Smit, M. E., Novák, O., Yamaguchi, N.,  
659 Yoshida, S., Van Isterdael, G., Palovaara, J., Nijse, B., Boekschoten, M. V., Hooiveld,  
660 G., Beeckman, T., Wagner, D., Ljung, K., Fleck, C., and Weijers, D. (2014). Integra-  
661 tion of growth and patterning during vascular tissue formation in *Arabidopsis*. *Science*,  
662 345:1255215.
- 663 Dupuy, L., Mackenzie, J., and Haseloff, J. (2010). Coordination of plant cell division and  
664 expansion in a simple morphogenetic system. *Proceedings of the National Academy of*  
665 *Sciences of the United States of America*, 107:2711–2716.
- 666 Errera, L. (1888). Über Zellformen und Siefenblasen. *Bottanisches Centralblatt*, 34:395–399.
- 667 Fowler, J. E. and Quatrano, R. S. (1997). Plant cell morphogenesis: plasma membrane in-  
668 teractions with the cytoskeleton and cell wall. *Annual Review of Cell and Developmental*  
669 *Biology*, 13:697–743.
- 670 Gibson, M. C., Patel, A. B., Nagpal, R., and Perrimon, N. (2006). The emergence of geometric  
671 order in proliferating metazoan epithelia. *Nature*, 442:1038–1041.
- 672 Gillies, T. E. and Cabernard, C. (2011). Cell division orientation in animals. *Current Biology*,  
673 21:R599–R609.
- 674 Graustein, W. C. (1931). On the average number of sides of polygons of a net. *Annals of*  
675 *Mathematics. Second Series*, 32(1):149–153.
- 676 Greig, D. M., Porteous, B. T., and Seheult, A. H. (1989). Exact maximum a posteriori estimation  
677 for binary images. *Journal of the Royal Statistical Society. Series B*, 51:271–279.

- 678 Grünbaum, B. (2003). *Convex Polytopes*. Number 221 in Graduate Texts in Mathematics.  
679 Springer-Verlag New York, second edition.
- 680 Hervieux, N., Tsugawa, S., Fruleux, A., Dumond, M., Routier-Kierzkowska, A.-L., Komat-  
681 suzaki, T., Boudaoud, A., Larkin, J. C., Smith, R. S., Li, C.-B., and Hamant, O. (2017).  
682 Mechanical shielding of rapidly growing cells buffers growth heterogeneity and contributes  
683 to organ shape reproducibility. *Current Biology*, 27:3468–3479.e4.
- 684 Hong, L., Dumond, M., Tsugawa, S., Sapala, A., Routier-Kierzkowska, A.-L., Zhou, Y., Chen,  
685 C., Kiss, A., Zhu, M., Hamant, O., Smith, R. S., Komatsuzaki, T., Li, C.-B., Boudaoud, A.,  
686 and Roeder, A. H. K. (2016). Variable cell growth yields reproducible organ development  
687 through spatiotemporal averaging. *Developmental Cell*, 38:15–32.
- 688 Hong, L., Dumond, M., Zhu, M., Tsugawa, S., Li, C.-B., Boudaoud, A., Hamant, O., and  
689 Roeder, A. H. K. (2018). Heterogeneity and robustness in plant morphogenesis: from  
690 cells to organs. *Annual Review of Plant Biology*, 69:469–495.
- 691 Korn, R. W. (1969). A stochastic approach to the development of coleocheate. *Journal of*  
692 *Theoretical Biology*, 24:147–158.
- 693 Legland, D., Arganda-Carreras, I., and Andrey, P. (2016). MorphoLibJ: integrated library and  
694 plugins for mathematical morphology with ImageJ. *Bioinformatics*, 32(22):3532–3534.
- 695 Lemke, S. B. and Nelson, C. M. (2021). Dynamic changes in epithelial cell packing during  
696 tissue morphogenesis. *Current Biology*, 31:R1098–R1110.
- 697 Lintilhac, P. M. and Vesecky, T. B. (1984). Stress-induced alignment of division plane in plant  
698 tissues grown in vitro. *Nature*, 307(5949):363–364.
- 699 Louveaux, M., Julien, J.-D., Mirabet, V., Boudaoud, A., and Hamant, O. (2016). Cell division  
700 plane orientation based on tensile stress in *Arabidopsis thaliana*. *Proceedings of the*  
701 *National Academy of Sciences of the United States of America*, 113(30):E4294–E4303.
- 702 Mansfield, S. G. and Briarty, L. G. (1991). Early embryogenesis in *Arabidopsis thaliana*. ii. the  
703 developing embryo. *Canadian Journal of Botany*, 69(3):461–476.
- 704 MATLAB (2012). *MATLAB and Statistics Toolbox Release 2012b (Version 8)*, The MathWorks,  
705 Inc. Natick, Massachusetts, United States.
- 706 Metropolis, N., Rosenbluth, A. W., Rosenbluth, M. N., Teller, A. H., and Teller, E. (1953).  
707 Equation of state calculations by fast computing machines. *Journal of Chemical Physics*,  
708 21(6):1087–1092.
- 709 Meyer, H. M. and Roeder, A. H. K. (2014). Stochasticity in plant cellular growth and patterning.  
710 *Frontiers in Plant Science*, 5:420.
- 711 Meyer, H. M., Teles, J., Formosa-Jordan, P., Refahi, Y., San-Bento, R., Ingram, G., Jönsson,  
712 H., Locke, J. C. W., and Roeder, A. H. K. (2017). Fluctuations of the transcription factor  
713 ATML1 generate the pattern of giant cells in the *Arabidopsis* sepal. *eLife*, 6.
- 714 Minc, N. and Piel, M. (2012). Predicting division plane position and orientation. *Trends in Cell*  
715 *Biology*, 22:193–200.

- 716 Moukhtar, J., Trubuil, A., Belcram, K., Legland, D., Khadir, Z., Urbain, A., Palauqui, J.-C., and  
717 Andrey, P. (2019). Cell geometry determines symmetric and asymmetric division plane  
718 selection in *Arabidopsis* early embryos. *PLoS Computational Biology*, 15:e1006771.
- 719 Moulia, B., Douady, S., and Hamant, O. (2021). Fluctuations shape plants through propriocep-  
720 tion. *Science*, 372.
- 721 Möller, B. K., Ten Hove, C. A., Xiang, D., Williams, N., López, L. G., Yoshida, S., Smit, M.,  
722 Datla, R., and Weijers, D. (2017). Auxin response cell-autonomously controls ground  
723 tissue initiation in the early *Arabidopsis* embryo. *Proceedings of the National Academy of  
724 Sciences of the United States of America*, 114:E2533–E2539.
- 725 Sahlin, P. and Jönsson, H. (2010). A modeling study on how cell division affects properties of  
726 epithelial tissues under isotropic growth. *PLoS ONE*, 5(7):e11750.
- 727 Schaefer, E., Belcram, K., Uyttewaal, M., Duroc, Y., Goussot, M., Legland, D., Laruelle, E.,  
728 de Tautzia-Moreau, M.-L., Pastuglia, M., and Bouchez, D. (2017). The preprophase  
729 band of microtubules controls the robustness of division orientation in plants. *Science*,  
730 356:186–189.
- 731 Scheres, B., Di Laurenzio, L., Willemsen, V., Hauser, M.-T., Janmaat, K., Weisbeek, P., and  
732 Benfey, P. N. (1995). Mutations affecting the radial organisation of the *Arabidopsis* root  
733 display specific defects throughout the embryonic axis. *Development*, 121(1):53–62.
- 734 Schindelin, J., Arganda-Carreras, I., Frise, E., Kaynig, V., Longair, M., Pietzsch, T., Preibisch,  
735 S., Rueden, C., Saalfeld, S., Schmid, B., Tinevez, J.-Y., White, D. J., Hartenstein, V.,  
736 Eliceiri, K., Tomancak, P., and Cardona, A. (2012). Fiji: an open-source platform for  
737 biological-image analysis. *Nature Methods*, 9:676–682.
- 738 Schütz, L. M., Louveaux, M., Vilches Barro, A., Bouziri, S., Cerrone, L., Wolny, A., Kreshuk, A.,  
739 Hamprecht, F. A., and Maizel, A. (2021). Integration of cell growth and asymmetric division  
740 during lateral root initiation in *Arabidopsis thaliana*. *Plant & Cell Physiology*, 62:1269–  
741 1279.
- 742 Soille, P. (2003). *Morphological Image Analysis: Principles and Applications*. Springer-Verlag,  
743 Berlin, Germany, second edition.
- 744 Truernit, E., Bauby, H., Dubreucq, B., Grandjean, O., Runions, J., Barthélémy, J., and Palauqui,  
745 J.-C. (2008). High-resolution whole-mount imaging of three-dimensional tissue organi-  
746 zation and gene expression enables the study of phloem development and structure in  
747 *Arabidopsis*. *The Plant Cell*, 20:1494–1503.
- 748 Vaddepalli, P., de Zeeuw, T., Strauss, S., Bürstenbinder, K., Liao, C.-Y., Ramalho, J. J., Smith,  
749 R. S., and Weijers, D. (2021). Auxin-dependent control of cytoskeleton and cell shape  
750 regulates division orientation in the *Arabidopsis* embryo. *Current Biology*, 31:4946–4955.
- 751 Vincent, L. and Soille, P. (1991). Watersheds in digital spaces: an efficient algorithm based on  
752 immersion simulation. *IEEE Transactions on Pattern Analysis and Machine Intelligence*,  
753 13(6):583–598.
- 754 Willis, L., Refahi, Y., Wightman, R., Landrein, B., Teles, J., Huang, K. C., Meyerowitz, E. M.,  
755 and Jönsson, H. (2016). Cell size and growth regulation in the *Arabidopsis thaliana* apical

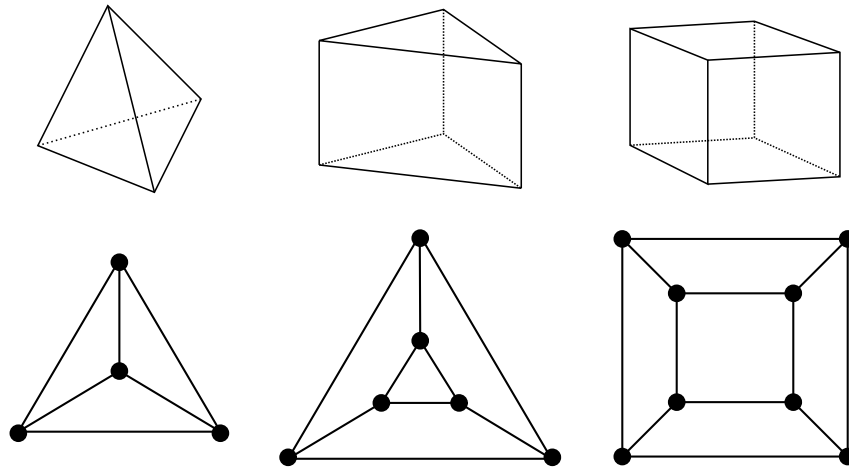
756 stem cell niche. *Proceedings of the National Academy of Sciences of the United States*  
757 *of America*, 113:E8238–E8246.

758 Wyatt, T. P. J., Harris, A. R., Lam, M., Cheng, Q., Bellis, J., Dimitracopoulos, A., Kabla, A. J.,  
759 Charras, G. T., and Baum, B. (2015). Emergence of homeostatic epithelial packing and  
760 stress dissipation through divisions oriented along the long cell axis. *Proceedings of the*  
761 *National Academy of Sciences of the United States of America*, 112:5726–5731.

762 Yoshida, S., Barbier de Reuille, P., Lane, B., Bassel, G. W., Prusinkiewicz, P., Smith, R. S.,  
763 and Weijers, D. (2014). Genetic control of plant development by overriding a geometric  
764 division rule. *Developmental Cell*, 29(1):75–87.

765 **Supplementary information: predicting the topology of ran-**  
766 **dom divisions using graph cuts on polyhedral graphs**

767 We consider the main three cell shapes observed during late embryogenesis in *Arabidopsis*  
768 *thaliana*. These shapes are the tetrahedron, triangular prism, and cuboid (containing 4, 5, and  
769 6 faces, 4, 6, and 8 vertices, and 6, 9, and 12 edges, respectively). Our objective here is to  
770 enumerate the different ways of dividing these cell shapes and to characterize the resulting  
771 daughter shapes. The key to our analysis is to represent cell shapes as planar polyhedral  
772 graphs and cell divisions as graph cuts on these polyhedral graphs.



Supplementary Figure S1: Polyhedral graphs for the three main cell shapes found in *Arabidopsis thaliana* early embryogenesis. Note that in these representations (Schlegel diagrams), the outside counts as one face of the corresponding polyhedron.

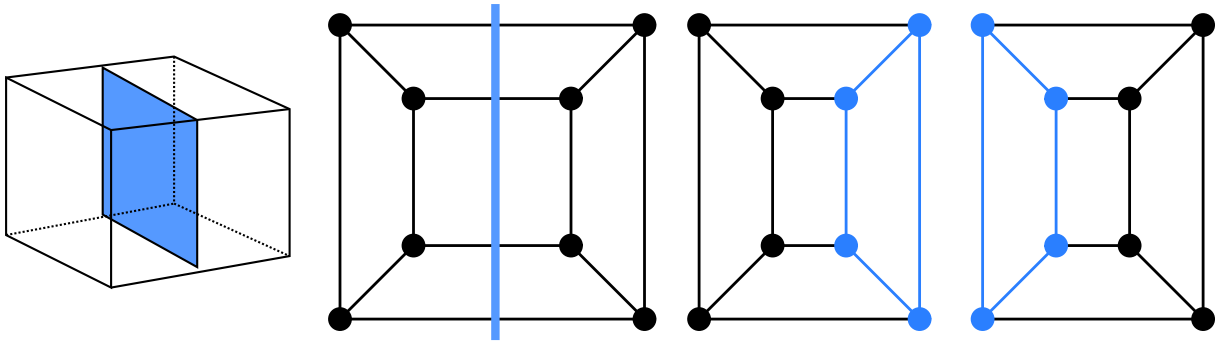
773 Any convex polyhedral cell shape with  $F$  faces can be represented by a 3-connected planar  
774 graph  $G$  of  $V$  vertices inter-connected by  $E$  edges (polyhedral graph). Such graphs can be  
775 represented in 2D by Schlegel diagrams (Figure S1). Because of the 3-connectivity of the  
776 corresponding graph, applying Euler's formula ( $V - E + F = 2$ ) to any of these shapes gives  
777 the following relations:

$$\begin{aligned}2E &= 3V \\2F &= 4 + V\end{aligned}$$

778 Hence, we only need to determine the number of vertices of the daughter cells to characterize  
779 a cell division in terms of the abstract resulting cell shapes.

780 Given that cell divisions avoid existing vertices, any division splits the cell vertices in two disjoint  
781 sets of vertices. These sets are non-empty because cell division planes extend from one face  
782 of the mother cell to another one. Cases where a division plane extends from an existing  
783 cell face to the same face are extremely rare and unknown in the embryo. Hence, a cell  
784 division corresponds to a graph cut, whereby a number of edges are removed to yield two  
785 disconnected subgraphs. Following cut, each subgraph is completed by adding new vertices  
786 at the cut positions. A new edge is also introduced for each pair of new vertices located on  
787 the same face of the mother cell. The two resulting graphs are the graphs of the two daughter  
788 cells (Figure S2). One consequence of representing cell division as a graph cut is that each  
789 face of the original mother cell is cut at most once. This implies that we do not consider curved  
790 division planes that would fold back to intersect a face more than once. This is consistent with  
791 biological observations in the plant embryo.

792 A division can be characterized by a couple of integers  $(p, q)$ , where  $p$  and  $q$  are the number  
793 of initial vertices that are separated by the division. Since  $q = V - p$ , the division is actually



Supplementary Figure S2: Cell division as cuts on polyhedral graphs: illustration with the division of a cuboid. The division on the left corresponds to the edge cut shown in the middle. Completing the two subgraphs of this cut with nodes and edges (*Blue*) yields the two subgraphs of the daughter cells. The obtained subgraphs correspond to two cuboids, as expected for the considered division.

794 fully characterized by  $p$  only. We call  $p$ -division a division that separates  $p$  vertices from the  
 795  $V - p$  other vertices ( $p > 0$ ). For example, the 1-divisions are the divisions whereby one of the  
 796 vertices is separated from all the other ones (“corner” division). Since the  $p$ -divisions and the  
 797  $q$ -divisions with  $q = V - p$  are two identical sets of divisions, we limit ourselves to situations  
 798 where  $p \leq q$ , i.e.,  $p \leq V/2$ .

799 We note  $N(p)$  the number of possible  $p$ -divisions of a given cell shape. For each of these  
 800 divisions, we note  $K(p)$  the number of removed edges (= size of the edge cut-set);  $V_p(p)$ ,  
 801  $E_p(p)$  and  $F_p(p)$  the total number of vertices, edges and faces in the daughter cell that inherits  
 802 the  $p$  vertices;  $V_q(p)$ ,  $E_q(p)$  and  $F_q(p)$  the total number of vertices, edges and faces in the  
 803 daughter cell that inherits the remaining  $q = V - p$  vertices;  $E_p^*(p)$  and  $E_q^*(p)$  the number of  
 804 edges that are inherited from the mother cell by each of these two daughter cells, respectively  
 805 (= number of edges in the subgraphs of  $G$  induced by the  $p$  and  $q$  vertices, respectively). We  
 806 derive below the expressions of all these quantities as functions of  $p$ .

807 Each edge cut creates a new vertex for each daughter cell. We thus have, for any  $p$ :

$$\begin{aligned} V_p(p) &= p + K(p) \\ V_q(p) &= q + K(p) \end{aligned}$$

808 Since each vertex is connected to three edges, the maximal number of possible cuts is  $3p$   
 809 (remember that  $p \leq q$ ). Each edge inherited by a daughter cell from its mother removes two  
 810 potential cuts (one for each end-vertex). This gives:

$$\begin{aligned} K(p) &= 3p - 2E_p^*(p) \\ &= 3q - 2E_q^*(p) \end{aligned}$$

811 We thus have:

$$\begin{aligned} V_p(p) &= 2 [2p - E_p^*(p)] \\ V_q(p) &= 2 [2q - E_q^*(p)] \end{aligned}$$

812 which we can write

$$\begin{aligned} V_p(p) &= 2Q_p(p) \\ V_q(p) &= 2Q_q(p) \end{aligned}$$

813 where

$$\begin{aligned} Q_p(p) &= 2p - E_p^*(p) \\ Q_q(p) &= 2q - E_q^*(p) \end{aligned}$$

814 This finally leads to the following simple expressions for the number of edges and faces in the  
815 daughter cells:

$$\begin{aligned} E_p(p) &= 3Q_p(p) \\ E_q(p) &= 3Q_q(p) \end{aligned}$$

816

$$\begin{aligned} F_p(p) &= 2 + Q_p(p) \\ F_q(p) &= 2 + Q_q(p) \end{aligned}$$

Given that

$$E = E_p^*(p) + E_q^*(p) + K(p)$$

we also have

$$Q_q(p) = V/2 + p - E_p^*(p)$$

817 In a graph-theoretical perspective, we can thus fully describe a  $p$ -division and the resulting  
818 daughter cell shapes by two parameters only: the number  $p$  of original vertices and the number  
819  $E_p^*(p)$  of original edges that are inherited by the “smallest” ( $p \leq q$ ) of the two daughter cells.

820 To go further we must distinguish two situations, depending on whether the subgraph induced  
821 by the  $p$  vertices and their  $E_p^*(p)$  edges is cyclic or not.

If the subgraph induced by the  $p$  vertices and their  $E_p^*(p)$  edges contains no cycle (this is systematically the case for  $p < 3$ ), then we have:

$$E_p^*(p) = p - 1$$

822 This gives the following features for a division induced by two acyclic subgraphs:

$$\begin{aligned} Q_p(p) &= p + 1 \\ Q_q(p) &= V/2 + 1 \\ V_p(p) &= 2(p + 1) \\ V_q(p) &= V + 2 \\ E_p(p) &= 3(p + 1) \\ E_q(p) &= 3V/2 + 3 \\ F_p(p) &= p + 3 \\ F_q(p) &= V/2 + 3 \end{aligned}$$

823 One corollary of these results is that:

$$\begin{aligned} F_p(p) &\leq F + 1 \\ F_q(p) &= F + 1 \end{aligned}$$

824 Hence, a division “in the acyclic case” systematically yields a daughter cell with one additional  
825 face compared with the mother. The other daughter cell has at most one additional face.

For the shapes we consider, we have  $p \leq 4$ . In this particular case, the presence of a cycle in the subgraph induced by the  $p$  vertices ( $p \geq 3$ ) and their  $E_p^*(p)$  edges necessarily leads to:

$$E_p^*(p) = p$$

826 which yields the following features for a division induced by a cyclic subgraph:

$$\begin{aligned} Q_p(p) &= p \\ Q_q(p) &= V/2 \\ V_p(p) &= 2p \\ V_q(p) &= V \\ E_p(p) &= 3p \\ E_q(p) &= 3V/2 \\ F_p(p) &= p + 2 \\ F_q(p) &= V/2 + 2 \end{aligned}$$

827 with, as a corollary, the following:

$$\begin{aligned} F_p &\leq F \\ F_q &= F \end{aligned}$$

828 Hence, a division in the “cyclic case” cannot generate shapes with a larger number of faces  
829 than the mother cell. In addition, one of the two daughter cells has systematically the same  
830 shape as the mother cell.

Now it remains to enumerate the number  $N(p)$  of different  $p$ -divisions for a given mother cell shape. The number of 1-divisions is simply:

$$N(1) = V$$

For the 2-divisions, we must distinguish the tetrahedral shape from the other ones because of symmetries of the 2-divisions in this shape:

$$N(2) = \begin{cases} E/2 & \text{if } V = 4 \\ E & \text{otherwise} \end{cases}$$

The number of 3-divisions (meaningful only for the two shapes with  $V \geq 6$ ) is the number of pairs of adjacent edges in the mother cell graph. There are three pairs of adjacent edges at each vertex. For the triangular prismatic shape, care must be taken that the two triangular faces induce symmetries. On each face, there are indeed three pairs of edges that define the same division (“cyclic” case). Hence we have

$$N(3) = \begin{cases} 3V - 5 & \text{if } V = 6 \\ 3V & \text{if } V = 8 \end{cases}$$

831 The 4-divisions are meaningful only for the cuboidal shape. They are obtained either by sepa-  
832 rating opposite quadrilateral faces of the mother cell (“cyclic” case) or by separating one vertex  
833 and its three connected neighbors from the other four vertices (“acyclic” case). Taking care of  
834 symmetries, we thus have:

$$\begin{aligned} N(4) &= F/2 + V/2 \\ &= 1 + \frac{3}{4}V \end{aligned}$$

$p/V - p$	1/3	2/2
$N(p)$	4	3
$p$ -shape	4.6.4	6.9.5
$q$ -shape	6.9.5	6.9.5

Table 1: Divisions of the tetrahedral cell shape (4.6.4).

835 Now we can compute the expected proportions of cell shapes resulting from the division of a  
 836 given cell shape, under a discrete uniform probability distribution over the space of possible  
 837 divisions. In the sequel, we refer to each shape by the triplet  $V.E.F$ .

The possible outcomes of the division of a tetrahedral (4.6.4) mother cell are given in Table 1. From this table, we obtain that the expected proportions of cell shapes following the division of a 4.6.4 cell are:

$$\text{Daughters of 4.6.4} \begin{cases} P(4.6.4) &= \frac{4}{14} & (28.6\%) \\ P(6.9.5) &= \frac{10}{14} & (71.4\%) \end{cases}$$

The possible outcomes of the division of a triangular prismatic (6.9.5) mother cell are given in Table 2. From this table, we obtain that the expected proportions of cell shapes following the division of a 6.9.5 cell are:

$$\text{Daughters of 6.9.5} \begin{cases} P(4.6.4) &= \frac{6}{56} & (10.7\%) \\ P(6.9.5) &= \frac{11}{56} & (19.6\%) \\ P(8.12.6) &= \frac{39}{56} & (69.9\%) \end{cases}$$

838 The possible outcomes of the division of a cuboidal (8.12.6) mother cell are given in Table 3.  
 839 From this table, we obtain that the expected proportions of cell shapes following the division of  
 840 a 8.12.6 cell are:

$$\text{Daughters of 8.12.6} \begin{cases} P(4.6.4) &= \frac{8}{90} & (8.9\%) \\ P(6.9.5) &= \frac{12}{90} & (13.3\%) \\ P(8.12.6) &= \frac{24}{90} & (26.7\%) \\ P(10.15.7) &= \frac{46}{90} & (51.1\%) \end{cases}$$

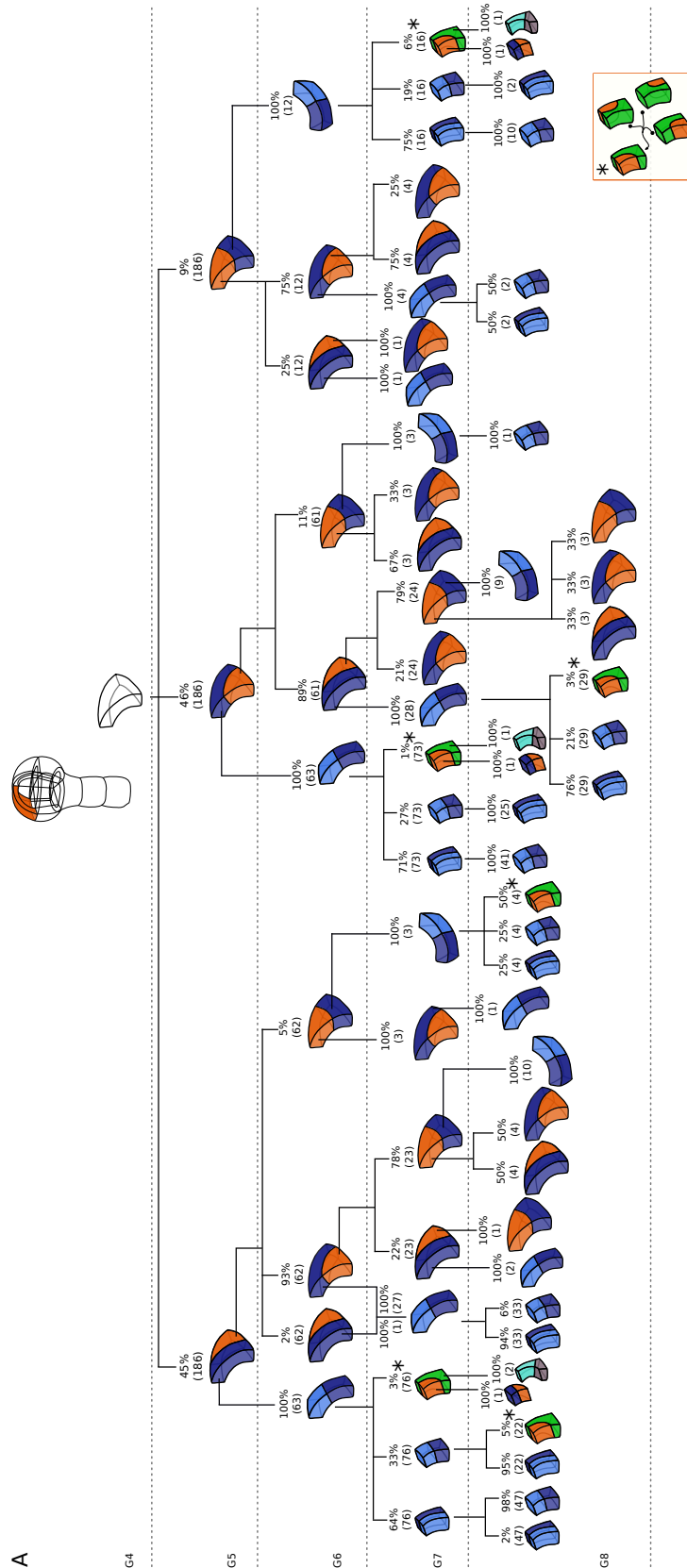
$p/V - p$	1/5	2/4	$3/3^\alpha$	$3/3^\beta$
$N(p)$	6	9	12	1
$p$ -shape	4.6.4	6.9.5	8.12.6	6.9.5
$q$ -shape	8.12.6	8.12.6	8.12.6	6.9.5

Table 2: Divisions of the triangular prismatic cell shape (6.9.5).  $\alpha$  refers to the case where the  $p$ -subgraph is acyclic,  $\beta$  to the case where it is cyclic.

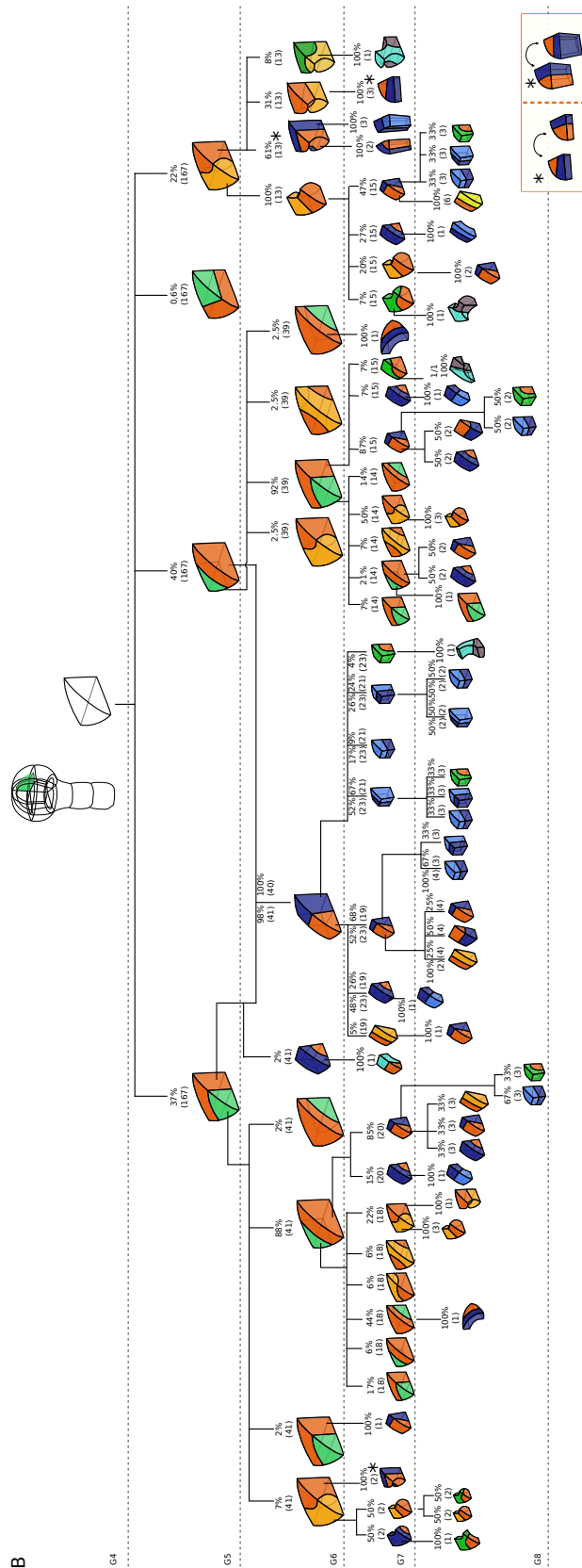
$p/V - p$	1/7	2/6	3/5	$4/4^\alpha$	$4/4^\beta$
$N(p)$	8	12	18	4	3
$p$ -shape	4.6.4	6.9.5	8.12.6	10.15.7	8.12.6
$q$ -shape	10.15.7	10.15.7	10.15.7	10.15.7	8.12.6

Table 3: Divisions of the cuboidal cell shape (8.12.6).  $\alpha$  refers to the case where the  $p$ -subgraph is acyclic,  $\beta$  to the case where it is cyclic.

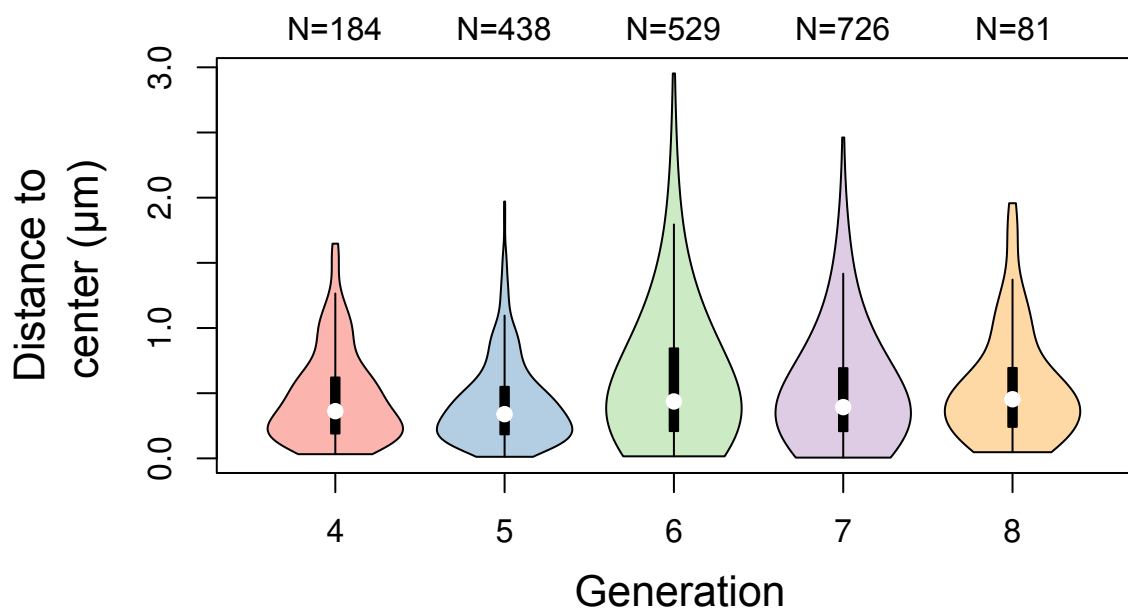
## 841 **Supplementary Figures**



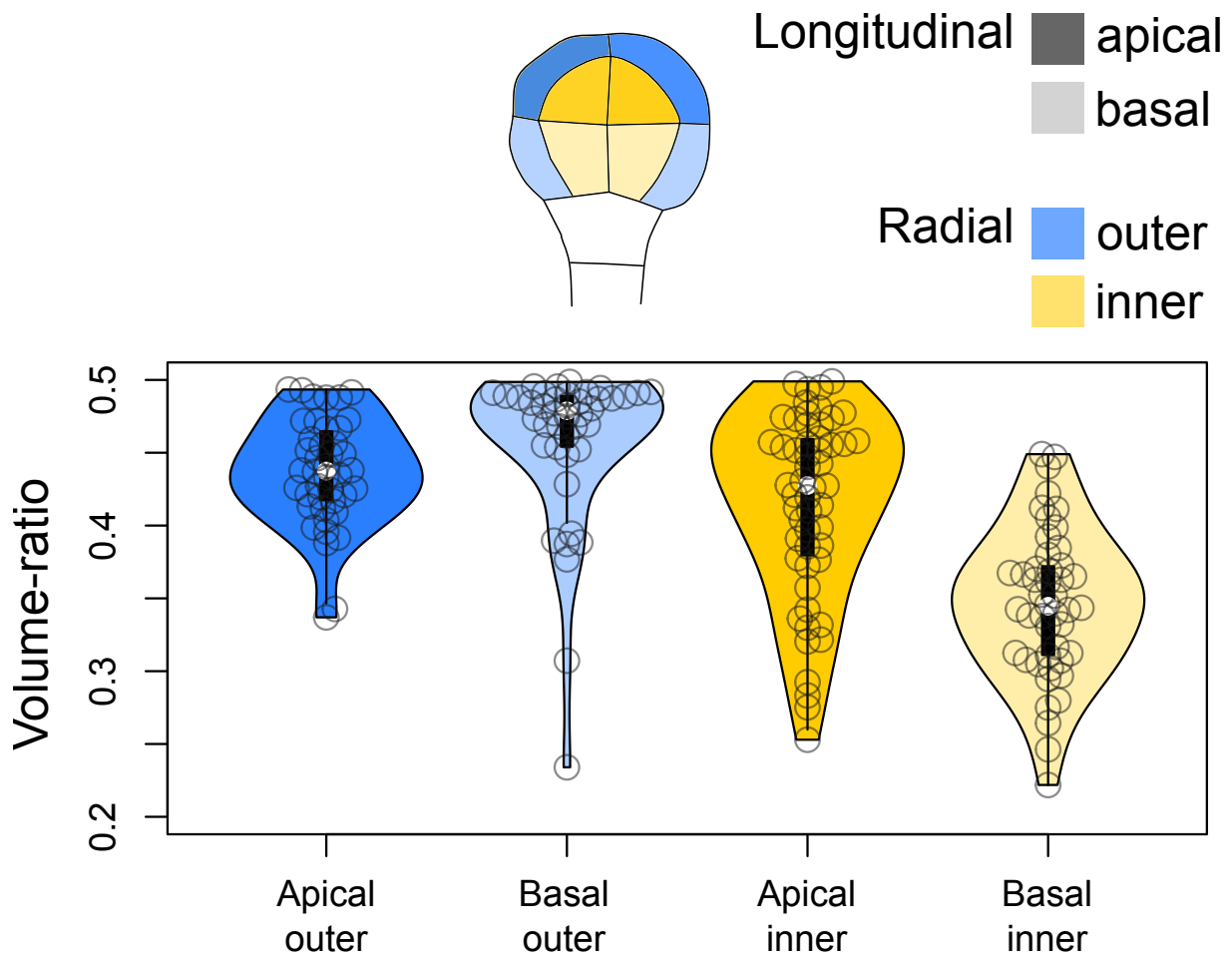
Supplementary Figure S3: Reconstructed cell lineages in the apical outer domain. Frequencies were computed based on observed patterns and patterns reconstructed at intermediate generations when rewinding lineages back to 16C stage from observed configurations. Numbers in parentheses are the total number of cases over which the percentages were calculated. Asterisks correspond to symmetrical alternatives that were not distinguished.



Supplementary Figure S4: Reconstructed cell lineages in the apical inner domain. Frequencies were computed based on observed patterns and patterns reconstructed at intermediate generations when rewinding lineages back to 16C stage from observed configurations. Numbers in parentheses are the total number of cases over which the percentages were calculated. Asterisks correspond to symmetrical alternatives that were not distinguished.

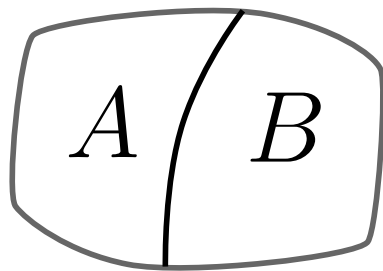


Supplementary Figure S5: Distance between cell division plane and cell center at different generations in *Arabidopsis thaliana* embryos. Distance was measured in mother cells reconstructed from identified sister cells at the immediately following generation.

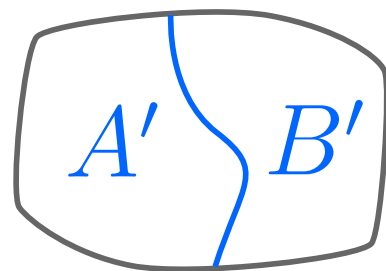
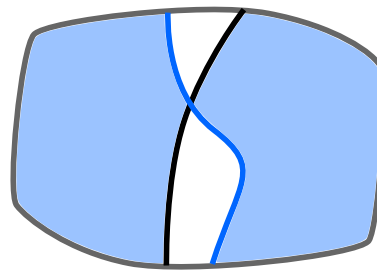


Supplementary Figure S6: Volume-ratio of cell divisions at the G4-G5 transition in the four embryo domains (shown at G4 above the graph). Volume-ratio of each division was computed as the ratio of cellular volumes between the smallest daughter cell and the mother cell.

Observed division

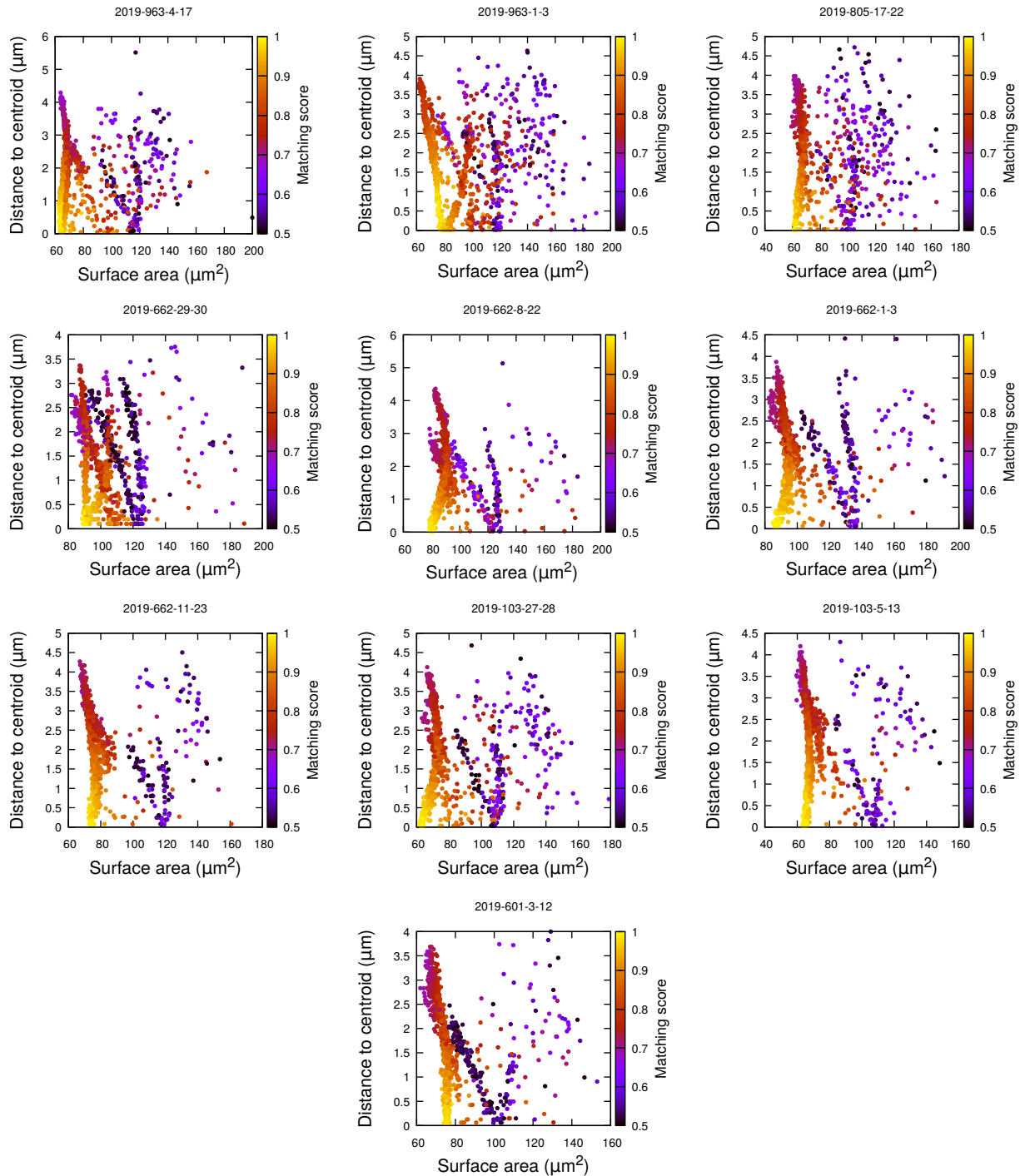


Matching

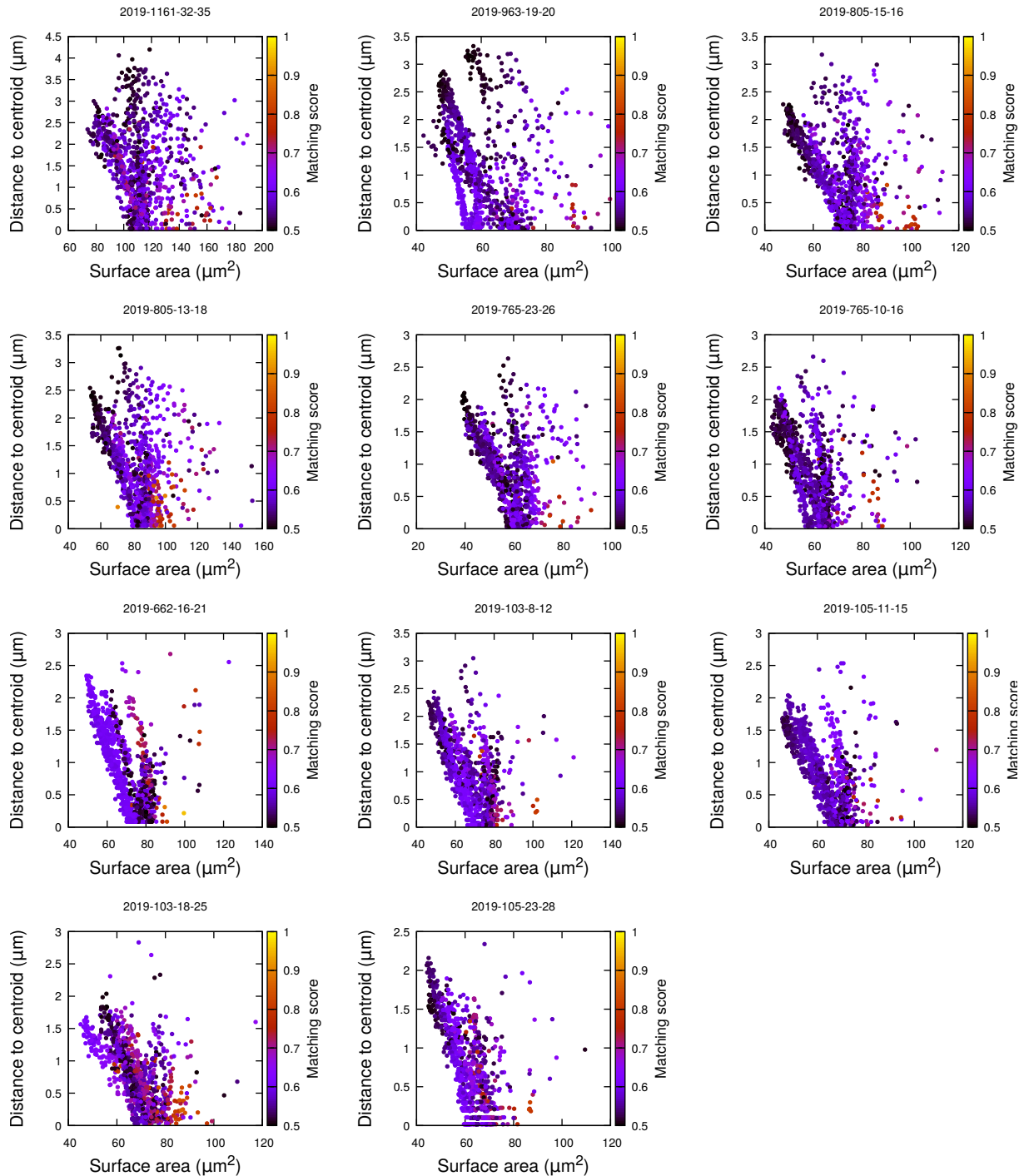


Simulated division

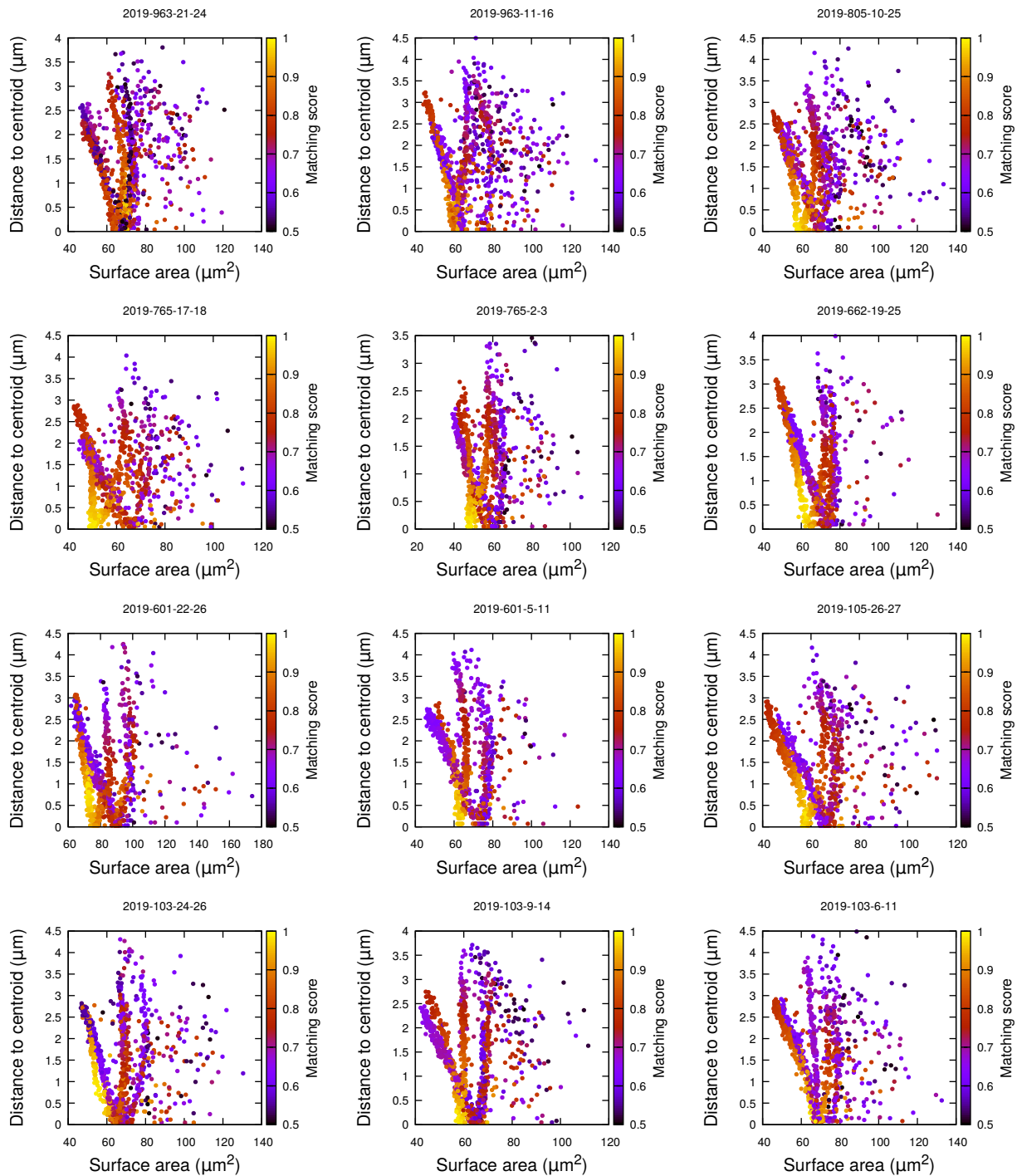
Supplementary Figure S7: Quantifying the similarity between observed and simulated cell divisions. The matching score is computed based on the maximum overlap between observed and daughter cells.



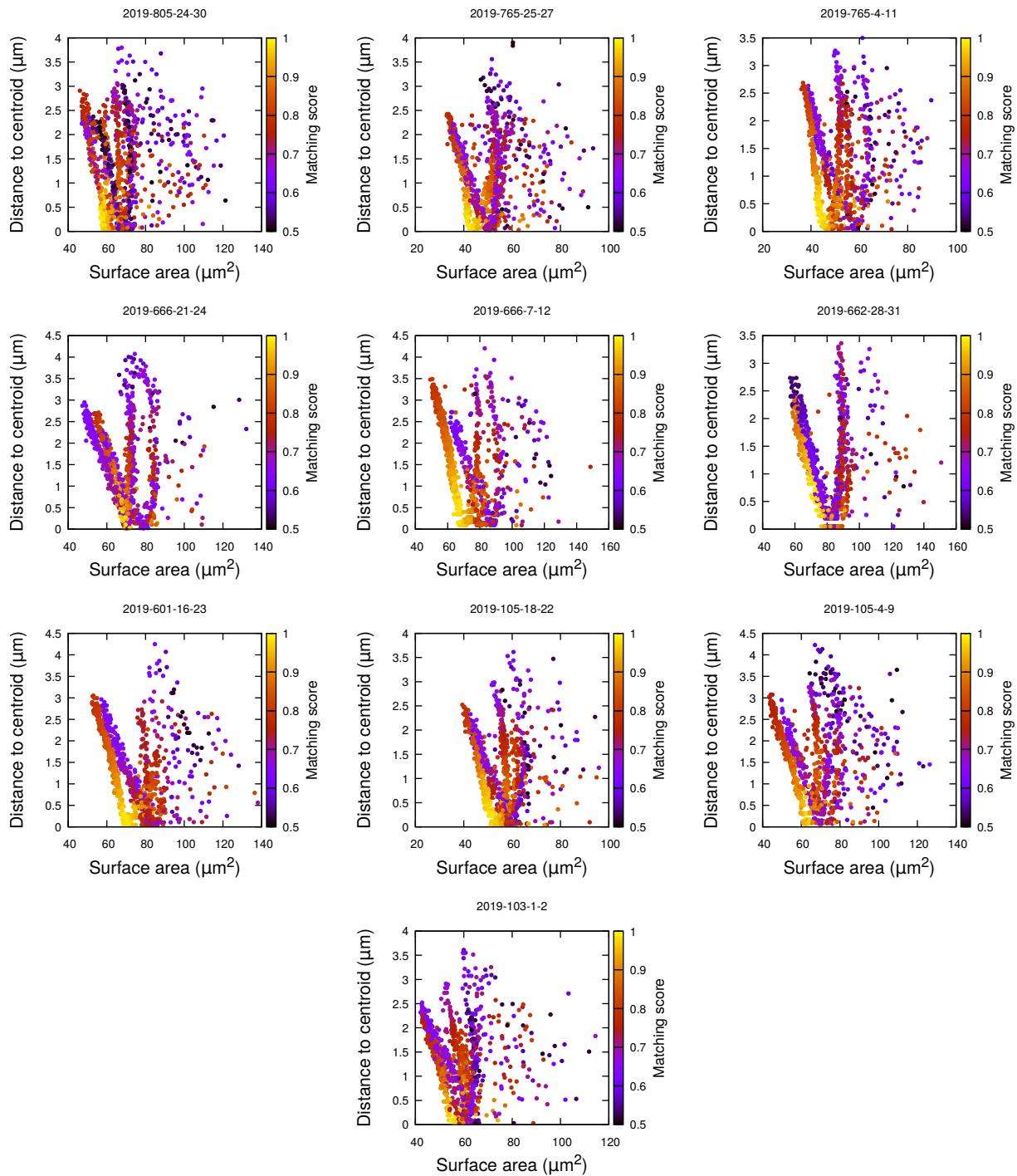
Supplementary Figure S8: Plane surface area and distance to cell center in simulations of cell divisions at the 16C-32C transition: the case of basal outer cells. Each plot corresponds to a mother cell at generation 4 that was reconstructed by merging two observed sister cells at generation 5. Each dot corresponds to a simulated division in the mother cell. One thousand simulations at arbitrary volume-ratios were performed in each mother cell. Colors indicate the degree of matching between simulations and observed divisions.



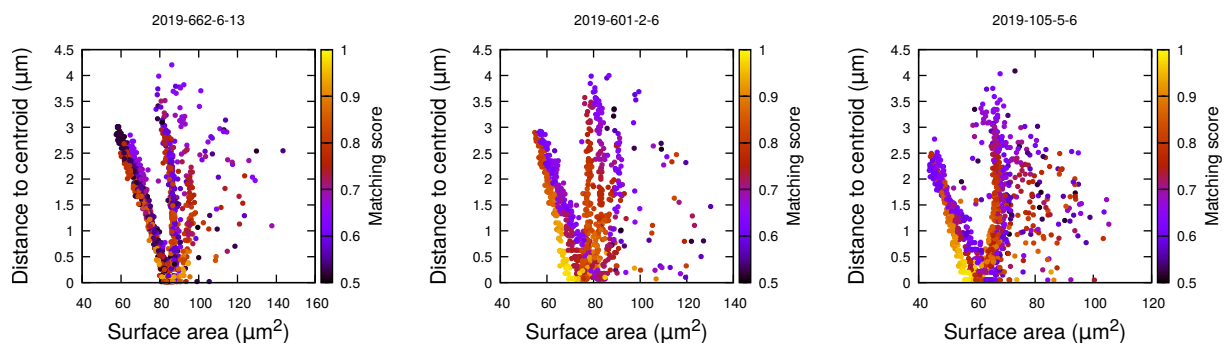
Supplementary Figure S9: Plane surface area and distance to cell center in simulations of cell divisions at the 16C-32C transition: the case of basal inner cells. Each plot corresponds to a mother cell at generation 4 that was reconstructed by merging two observed sister cells at generation 5. Each dot corresponds to a simulated division in the mother cell. One thousand simulations at arbitrary volume-ratios were performed in each mother cell. Colors indicate the degree of matching between simulations and observed divisions.



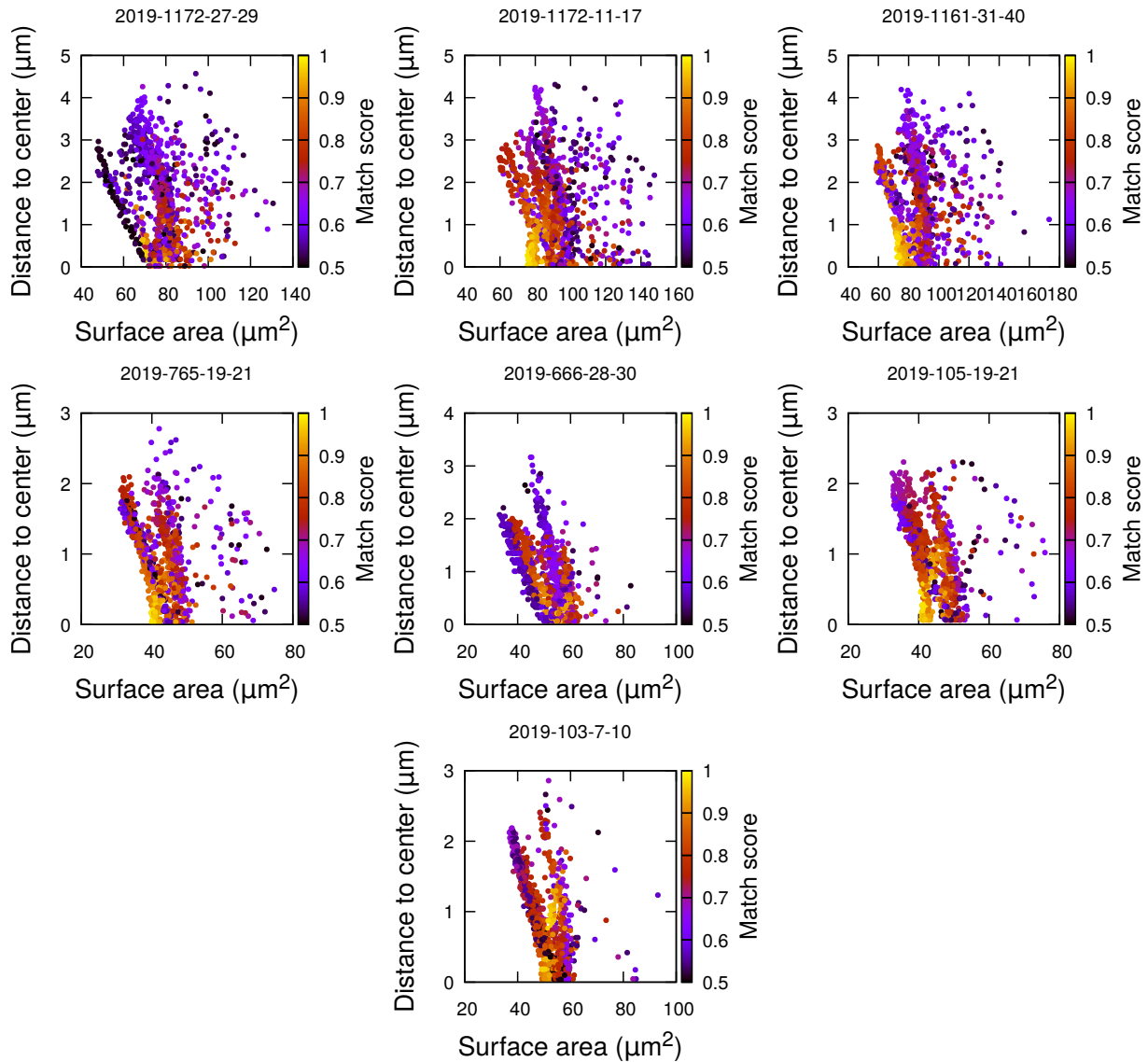
Supplementary Figure S10: Plane surface area and distance to cell center in simulations of cell divisions at the 16C-32C transition: the case of apical external cells dividing with a cuboid to the left. Each plot corresponds to a mother cell at generation 4 that was reconstructed by merging two observed sister cells at generation 5. Each dot corresponds to a simulated division in the mother cell. One thousand simulations at arbitrary volume-ratios were performed in each mother cell. Colors indicate the degree of matching between simulations and observed divisions.



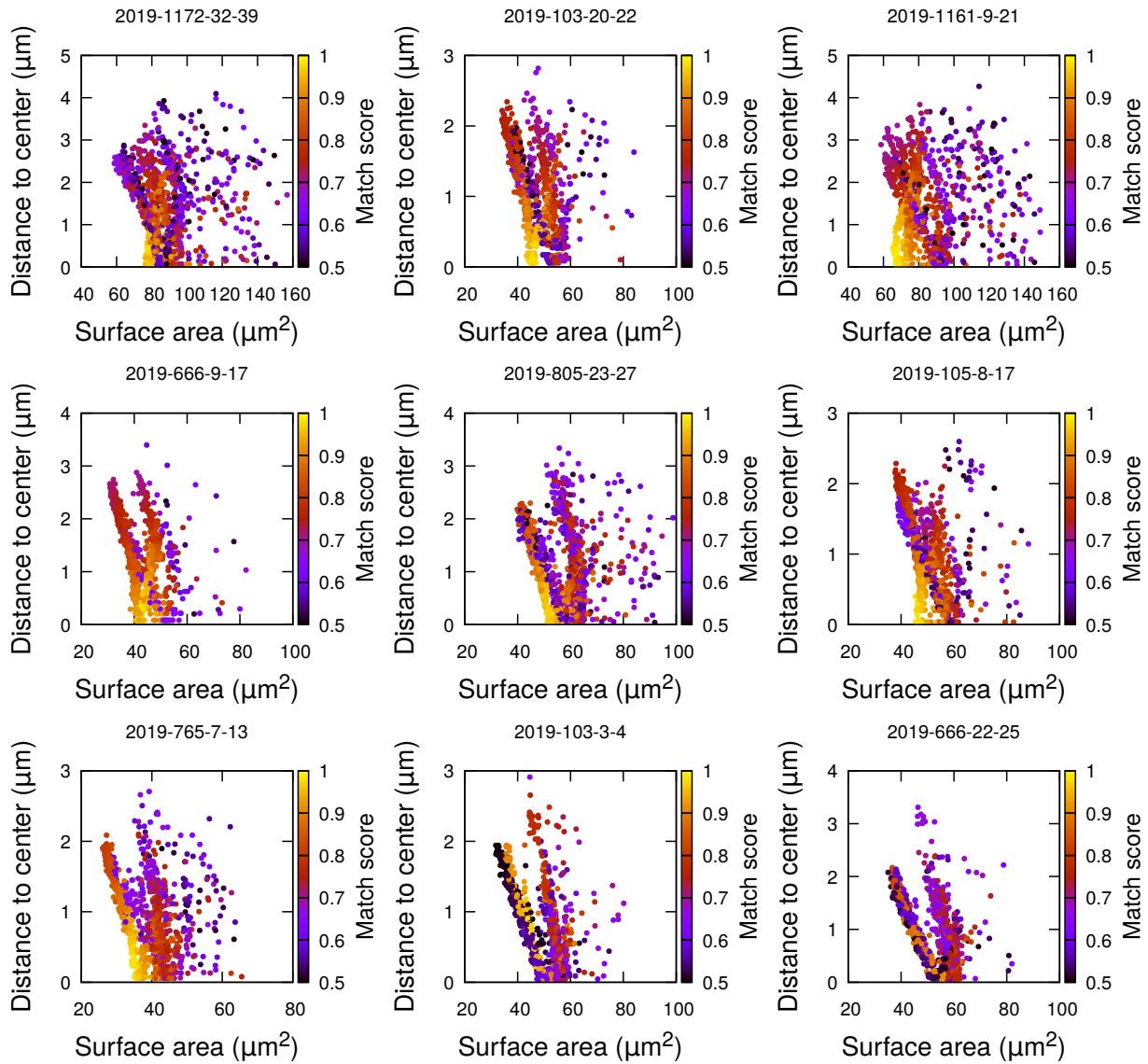
Supplementary Figure S11: Plane surface area and distance to cell center in simulations of cell divisions at the 16C-32C transition: the case of apical external cells dividing with a cuboid to the right. Each plot corresponds to a mother cell at generation 4 that was reconstructed by merging two observed sister cells at generation 5. Each dot corresponds to a simulated division in the mother cell. One thousand simulations at arbitrary volume-ratios were performed in each mother cell. Colors indicate the degree of matching between simulations and observed divisions.



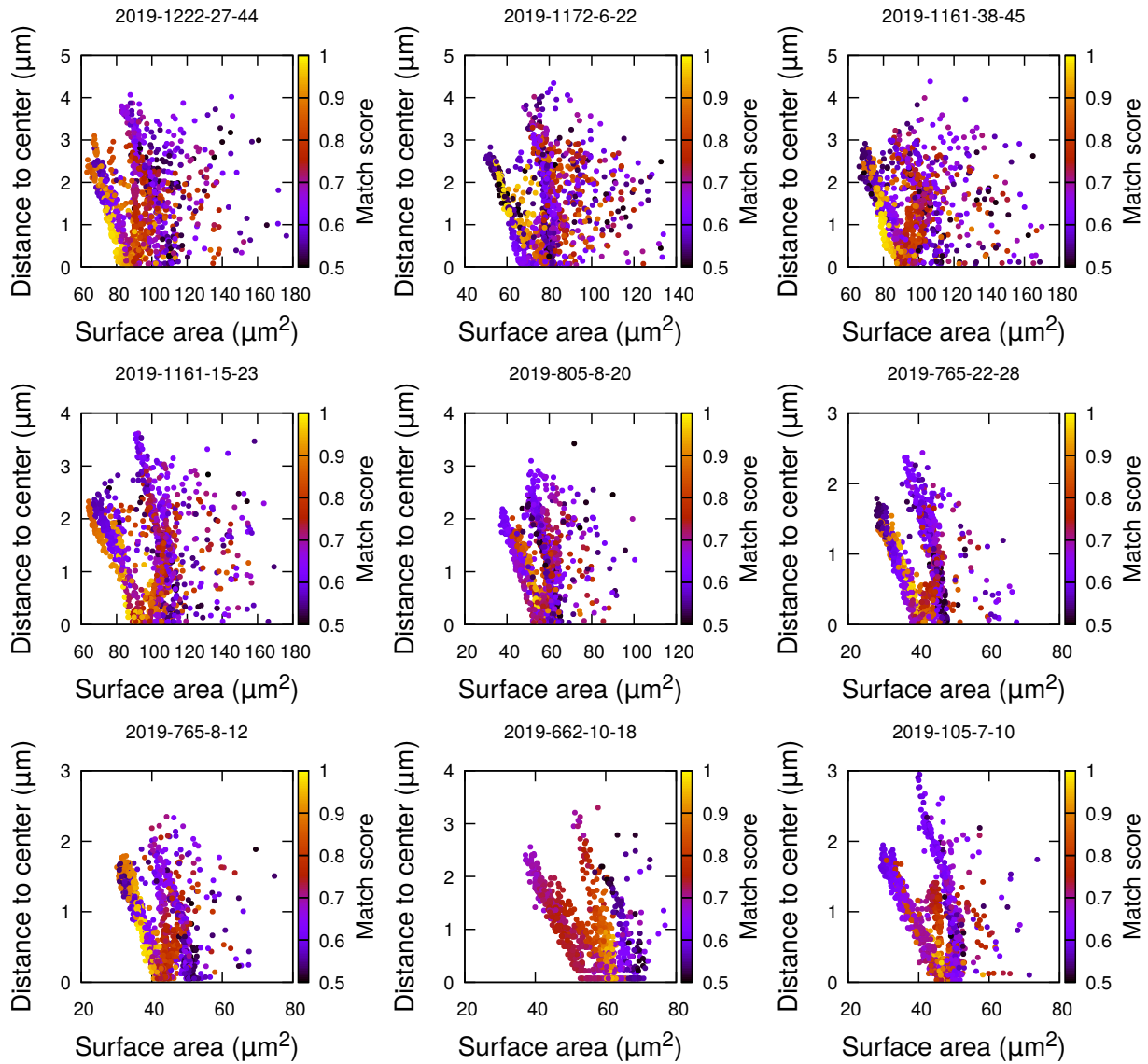
Supplementary Figure S12: Plane surface area and distance to cell center in simulations of cell divisions at the 16C-32C transition: the case of apical external cells dividing transversely. Each plot corresponds to a mother cell at generation 4 that was reconstructed by merging two observed sister cells at generation 5. Each dot corresponds to a simulated division in the mother cell. One thousand simulations at arbitrary volume-ratios were performed in each mother cell. Colors indicate the degree of matching between simulations and observed divisions.



Supplementary Figure S13: Plane surface area and distance to cell center in simulations of cell divisions at the 16C-32C transition: the case of apical internal cells dividing with a triangular prism to the left. Each plot corresponds to a mother cell at generation 4 that was reconstructed by merging two observed sister cells at generation 5. Each dot corresponds to a simulated division in the mother cell. One thousand simulations at arbitrary volume-ratios were performed in each mother cell. Colors indicate the degree of matching between simulations and observed divisions.



Supplementary Figure S14: Plane surface area and distance to cell center in simulations of cell divisions at the 16C-32C transition: the case of apical internal cells dividing with a triangular prism to the right. Each plot corresponds to a mother cell at generation 4 that was reconstructed by merging two observed sister cells at generation 5. Each dot corresponds to a simulated division in the mother cell. One thousand simulations at arbitrary volume-ratios were performed in each mother cell. Colors indicate the degree of matching between simulations and observed divisions.



Supplementary Figure S15: Plane surface area and distance to cell center in simulations of cell divisions at the 16C-32C transition: the case of apical internal cells dividing longitudinally and radially. Each plot corresponds to a mother cell at generation 4 that was reconstructed by merging two observed sister cells at generation 5. Each dot corresponds to a simulated division in the mother cell. One thousand simulations at arbitrary volume-ratios were performed in each mother cell. Colors indicate the degree of matching between simulations and observed divisions.